A comparative analysis of several models of the ventricular depolarisation : introduction of a string model

th e

A COMPARATIVE ANALYSIS OF SEVERAL MODELS OF THE VENTRICULAR DEPOLARISATION; INTRODUCTION OF A STRING MODEL

by

Ir. A.A.H. Damen

Group Measurement and Control
Department of Electrical Engineering
Eindhoven University of Technology
Eindhoven, The Netherlands

A COMPARATIVE ANALYSIS OF SEVERAL MODELS OF THE VENTRICULAR DEPOLARISATION; INTRODUCTION OF A STRING MODEL.

BY

Ir. A.A.H. Damen

T.H. Report 73-E-41

October 1973

ISBN 90 6144 041 6

Contents

Abstract

The familiar one dipole, multiple dipole and multipole models of the electric heart action are tested on their suitability of simulating the field of double layers, which change in time. These double layers form part of a new model (string model) of the depolarisation wave through the heart ventricles based on a gross physiological resemblance.
The string model consists of two strings of dipoles, that travel along the endocardium; the depolarisation of the myocardium is represented by "filters" responding to the dipoles.
If the well known models fail in a model-to-model test with the string model, it is to be expected, that they also can not handle the more complex real situation.
Furthermore the string model itself may provide an expedient for tackling the so called direct and inverse problem of electrocardiography.

Introduction

In the past many models have been developed for describing the depolarising action in the ventricles of the heart and the consequent potentials in electrodes on the body surface. The oldest model, a fixed dipole with variable direction and strength as a function of time, is generally known. Geselowitz (ref. 1) improved this model by adding higher order poles, which resulted in a so called *multipole expansion*. In practice models of this kind could simulate electrode signals up to a high extent.

Because models were desired, in which more correlation exists with the physical phenomenon of the depolarisation wave, the *multidipole model* was introduced by e.g. Selvester (ref. 2, 3). (See also ref. 4, 5, 6, 7, 8, 9).

For an impression of the total information provided by the electrode signals, the model of the *intrinsic components* is also frequently used (ref. 10, 11, 12). All these models have one feature in common: the electrode potentials are always described by

$$\Phi(\underline{r}, t) = \underline{a}^T(\underline{r})\ \underline{f}(t)$$

where Φ is the potential in an electrode as a function of time t and the position of the electrode $\underline{r}$. The vector $\underline{a}$ is a function of only $\underline{r}$, whereas $\underline{f}$ is a vector function of the time only. Considerations about the quasi-stationarity can be found in ref. 13. In the one dipole model the f(t) represents the dipole components and in the multipole expansion the f(t) equals the coëfficients a_{nm} and b_{nm} (see section 3). In the multidipole model the $f_i(t)$ is the strength of dipole i. At last the $f_i(t)$ can be an intrinsic component. The vector $\underline{a}$ is mainly defined by the medium in between the heart and the electrodes, while the f(t) is directly dependent on the depolarisation wave. Sometimes the $\underline{a}$ becomes a function of time, when e.g. the origin of the one dipole model changes in time. In that case three extra time functions have to be introduced.

The number of time functions, mainly $f_i(t)$, can be considered as a criterion for the extent of a model. With that criterion the models mentioned above can be compared in their ability of simulating electrode potentials. The research, which is reported here, deals with this aspect.

It is clear then, that a reference model is needed, which does not discretise the depolarisation wave by a small number of dipoles or multipoles.

A continuous model of the depolarisation wave is preferred. This continuous model, (which we will name string model for reasons which will become clear later on) is described in sections 2 and 3, while in section 1 some marginal notes about it are made.
Sections 4 till 9 are dedicated to a comparison of the several models.

1. The objective of the string model.

A mathematical model of the depolarisation wave is proposed, which explains the essential part of the true depolarisation wave as far as some phenomena are concerned, that have been noted in literature, but not yet explained satisfactorily. These phenomena include the following:

1) The equivalent dipole model simulates the ECG signals up to a high degree of accuracy.
2) Three (or even two) intrinsic components (ref. 10, 11, 12) are predominant. Of course this fact highly correlates with the first phenomenon.

In other studies explanations for these observations have been sought in the medium, surrounding the heart muscle such as the intracavitary blood mass, the lungs and the physical boundary of the body. (ref. 14, 15, 16, 17, 18). In the research on which is reported here, however, the attention is concentrated on the heart itself and an attempt is made to establish a model, which accounts for the progression of the electrical field in time as well. Consequently the model can be used to relate the frequency contents of the electrode signals on the one side and local speeds of the propagation of the depolarisation wave combined with the geometry of the heart muscle on the other side.

Before entering into details about the model it is useful to emphasize, that it is by no means the objective to develop a model, which exactly represents the depolarisation wave. This would be impossible both due to insufficient knowledge and due to the fact, that appreciable differences are to be expected between individual depolarisation waves. This holds for the variability between humans as well as for differences with the depolarisation of dogs' hearts, which are a predominant source of experimental knowledge. Most attention is paid to the essential course of the depolarisation wave as it has been measured, e.g. ref. 19, 20, 21, 22, 23.

The shape of the heart is also strongly simplified in order to facilitate mathematical operations. In spite of these simplifications the confidence remains, that the model chosen shares with the heart the main field properties and also possesses so much flexibility, that improvements in details can easily be performed. Furthermore an important aspect is, that the models, used until now, such as the *equivalent dipole*, the *multipole* and the *multiple dipole model* can be compared directly with this new model, especially in their resemblance of surface potentials.

2. The physiological background of the string model.

The main course of the depolarisation wave is from the A.V. node by way of the bundle of His and the Purkinje fibers into the heart muscle. The myocardium is stimulated by the Purkinje fibers and the first depolarisation takes place more or less in the middle of the septum in two points, one on the left ventricle side and the other on the right ventricle side. The conduction in the septum behaves as though the left and right ventricles possess own separated walls. The depolarisation wave starts at the ventricle sides and is then directed towards the inside of the septum.

Next there is a fast propagation in the endocardium because of the Purkinje fibers situated there and from this endocardium the depolarisation wave proceeds through the myocardium towards the epicardium. This behaviour of the depolarisation wave suggests to model first the endocardium activity and secondly the myocardium activity, which is triggered by the former activity.

In order to facilitate calculations the anatomy of the heart is reduced to a simple sterometrical configuration. For that purpose the ventricle walls and the septum are supposed to be infinitisimally thin. The dimension of the musculature is accounted for later on. Moreover these walls have the shape of a sphere of radius R truncated by a flat plane, the base. In this truncated sphere a flat plane, perpendicular to the base and passing through the center of the sphere, represents the septum. For the sake of representation and calculation it is advisable to use a coordinate system like sketched in figure 1.

First we like to model the depolarisation front in the endocardium of the left ventricle.

At time $t = 0$, the beginning of the QRS-complex, the septum is activated in the origin. A small time Δt later the depolarisation is propagated in the x-y-plane equally in all directions by way of the Purkinje fibers so that the front can be supposed to look like a circle. This circle is concentric with the sphere and has a radius equal to $r_c = v_e.\Delta t$, where v_e is the propagation speed in the Purkinje fibers. This circular depolarisation front proceeds until the base is reached at $t = t_1$, after which the circle reduces to an arc of a circle up to the base.

At $t = t_2$ the sphere surface is reached and the depolarisation front moves like an arc of a circle along the sphere, whereby

$$\psi = \frac{v_e.(t-t_2)}{R} = \frac{v_e.t}{R} - 1$$

(see figure 1)

At time $t = t_3$ the arc passes into a complete circle again and at $t = t_4$ the depolarisation front ends on the z-axis for $z = R$.
The same holds equally for the depolarisation front in the endocardium of the right ventricle. From the endocardium the depolarisation is conducted through the myocardium towards the epicardium.
This propagation is modelled by a current dipole string on the depolarisation fronts in the endocardium, directed outwards and acting during the time, that the depolarisation wave needs to reach the epicardium (see figure 2).
This duration T is equal to d/v_1, where d is the local thickness of the heart wall and v_1 is the propagation speed through the myocardium. As a first approximation we distinguish four parts of the heart with different thickness, viz.:

d_L = thickness of the outside wall of the left ventricle
d_R = thickness of the outside wall of the right ventricle
d_{LS} = thickness of the septum part belonging to the left ventricle
d_{RS} = thickness of the septum part belonging to the right ventricle

The evaluation of the electrical field in the medium outside the heart can be seen as a time filtering of a rather simple dipole string model, which represents the depolarisation fronts in the endocardium. For each of the heart parts mentioned above a dipole string can be placed on the depolarisation front of the endocardium. The field due to this dipole string can be evaluated for an infinite, homogeneous and isotropic medium. The thickness of the local heart wall is then brought in by *filtering* this potential in time by a filter, which has a rectangular impulse response, like indicated in figure 3. Another interpretation is a dipole string which is triggered by the endocardium and is maintained by the myocardium during a time proportional to the local thickness of the myocardium. The effect of this operation is, that the resulting potentia is originated by a homogeneous current dipole layer in the form of a ribbon in between the depolarisation fornt circles at time t and t - T.
Figure 4 gives a picture of the situation of the depolarisation wave at several moments. The constants for that special case are given in table 1, whereas more information about detailed calculations will be given in section 3.

Naturally, the above theory is based on the assumption of a quasistationary field. After the filtering of the different parts has been performed, the resulting potentials can be summed on account of the superposition theorem. Because of the use of dipole strings we name the above model, the *string model.*

Some supplementary remarks have to be made.

At time t_2 the direction of the dipole string is suddenly rotated over 90 degrees. This phenomenon is exaggerated because the depolarisation wave has been started exactly in the middle of the septum in order to facilitate calculations. In the real situation the depolarisation starts somewhere on the positive x-axis. Then the depolarisation front does not end on the z-axis, but somewhere in the quadrant $x < 0 \quad z > 0$. In this situation the moment t_2 of the rotation of the dipole directions is not sharply defined but spread over a small interval time. Nevertheless the sudden change will probably result in the fast change of the VCG at the beginning of the R-wave.

This effect is enlarged by the high activity of the apex. In this part of the heart the walls of the ventricles are thick. This property however is only partially incorporated in our model.

This discrepancy with the real situation is one of the main differences with reality. We made three assumptions:

1) The septum is a flat plane with a circular boundary.
2) The depolarisation front starts in the center of the septum.
3) The depolarisation propagates uniformly because of the homogeneous spread of Purkinje fibers.

None of these three conditions is fully satisfied.

Therefore the depolarisation front will not reach the outside walls everywhere at the same time. On the contrary, according to Durrer (ref. 20) the break-through takes place in the anterior special wall of the right ventricle and the posterior wall of the left ventricle somewhere between the apex and the base.

Furthermore, because of the inhomogeneous spread of Purkinje fibers, the conduction in the basical parts of the septum and the right ventricle is low. This implies, that the depolarisation ends in these heart segments. Then the depolarisation wave in the septum is directed towards the base and the direction of the final depolarisation front in the right ventricle wall possesses also an important tangential component.

Another assumption is the pure radial direction of the depolarisation wave. The direction of the dipole layer is always taken perpendicular to the walls, whereas the tangential component is neglected. As far as this aspect is concerned we refer to the so called Brody effect caused by the intracavitary blood mass (see ref. 14).

3. Evaluation of the field potential

Before the "filtering action" is performed, the potential is due to two strings of dipoles in the form of an arc or a circle. $\underline{m}$ defines the dipole intensity per length in each direction and $\underline{p}$ defines the position of a small part of the string. If $\underline{r}$ is the position of the observation point, then

$$\phi^* = 4\pi\sigma V^* = \int \frac{\underline{m}^T(\underline{r}-\underline{p})}{|\underline{r}-\underline{p}|^3}\, dl = \int \underline{m}^T \nabla_{\underline{p}} \left(\frac{1}{|\underline{r}-\underline{p}|}\right) dl \qquad (1)$$

where V^* is the true potential

ϕ^* is a normalised potential, which we will generally use.

σ is the specific conductivity

the integration is performed over the dipole string.

The use of a multipole expansion in spherical coordinates is suggested both by the spherical geometry of the model and the frequent use of this expansion in literature, e.g. ref. 1, 15, 18, 24, 25, 26, 27, 28.

Let

$$\underline{r} = r \begin{bmatrix} \sin\theta_r \cos\phi_r \\ \sin\theta_r \sin\phi_r \\ \cos\theta_r \end{bmatrix} \qquad \underline{p} = p \begin{bmatrix} \sin\theta_p \cos\phi_p \\ \sin\theta_p \sin\phi_p \\ \cos\theta_p \end{bmatrix}$$

then

$$\frac{1}{|\underline{r}-\underline{p}|} = \frac{1}{r} \sum_{n=0}^{\infty} \sum_{m=0}^{n} \left(\frac{p}{r}\right)^n (2-\delta_m^o) \frac{(n-m)!}{(n+m)!} P_n^m(\cos\theta_r) P_n^m(\cos\theta_p) \cos m(\phi_r-\phi_p)$$

where P_n^m are associated Legendre functions of the first kind,

and $$\delta_m^o = \begin{cases} 1 & \text{if } m = 0 \\ 0 & \text{if } m \neq 0 \end{cases}$$

see e.g. ref. 1, 25

If this expansion is uniformly convergent, summation and integration or differentiation may be interchanged.
For determining the gradient we use the chain rule:

$$\nabla_{\underline{p}}\left(\frac{1}{|\underline{r}-\underline{p}|}\right)=\frac{\partial\left(\frac{1}{|\underline{r}-\underline{p}|}\right)}{\partial p}\nabla_{\underline{p}}(p)+\frac{\partial\left(\frac{1}{|\underline{r}-\underline{p}|}\right)}{\partial\theta_p}\nabla_{\underline{p}}(\theta_p)+\frac{\partial\left(\frac{1}{|\underline{r}-\underline{p}|}\right)}{\partial\phi_p}\nabla_{\underline{p}}(\phi_p)$$

Substitution in integral (1) results in:

$$\phi^* = \frac{1}{r}\sum_{n=1}^{\infty}\sum_{m=o}^{n}\frac{1}{r^n}P_n^m(\cos\theta_r)\left\{a_{nm}^*\cos m\phi_r + b_{nm}^*\sin m\phi_r\right\}$$

where

$$\left\langle \begin{matrix} a_{nm}^* \\ b_{nm}^* \end{matrix} \right\rangle = (2-\delta_m^o)\frac{(n-m)!}{(n+m)!}\int\left\{ p^{n-1}\underline{m}^T \right.$$

$$nP_n^m(\cos\theta_p)\begin{bmatrix}\sin\theta_p\cos\phi_p\\ \sin\theta_p\sin\phi_p\\ \cos\theta_p\end{bmatrix}\left\langle \begin{matrix}\cos m\phi_p\\ \sin m\phi_p\end{matrix}\right\rangle +$$

$$\frac{\partial P_n^m(\cos\theta_p)}{\partial\theta_p}\begin{bmatrix}\cos\theta_p\cos\phi_p\\ \cos\theta_p\sin\phi_p\\ -\sin\theta_p\end{bmatrix}\left\langle \begin{matrix}\cos m\phi_p\\ \sin m\phi_p\end{matrix}\right\rangle +$$

$$\left. P_n^m(\cos\theta_p)\begin{bmatrix}-\sin\phi_p/\sin\theta_p\\ \cos\phi_p/\sin\theta_p\\ 0\end{bmatrix}\left\langle \begin{matrix}-m\sin m\phi_p\\ m\cos m\phi_p\end{matrix}\right\rangle \right\}\,dl \qquad (2)$$

Now it is easy to recognize the multipole expansion where n denotes the order of the multipole.
Above expressions for a_{nm}^* and b_{nm}^* look quite complicated. Application to our configuration, however, results in simple formula's. Because of the symmetry with respect to the x-z plane, all b_{nm}^* are zero.

As an example we will evaluate the activity of the left ventricle:

for $t \leq t_2$

$$\underline{m} = \begin{bmatrix} 0 \\ 0 \\ -1 \end{bmatrix} \qquad \underline{p} = r_c \begin{bmatrix} \cos\phi \\ \sin\phi \\ 0 \end{bmatrix} \qquad \begin{aligned} r_c &= v_e.t \\ \theta_p &= \pi/2 \end{aligned}$$

Substitution in (2) results in:

$$\text{if } m = 0 \text{ then } a^*_{no} = \begin{cases} 0 & \text{for n even} \\ 2(-1)^{\frac{n+1}{2}} \dfrac{1.3.5....n}{2.4.6....(n-1)} \phi_{max} r_c^n & \text{for n odd} \end{cases}$$

$$\text{if } m \neq 0 \text{ then } a^*_{nm} = \begin{cases} 0 & \text{for m + n even} \\ (-1)^{\frac{n-m+1}{2}} \dfrac{4}{m} \dfrac{1.3.5....(n-m)}{2.4.6....(n+m-1)} r_c^n \sin(m\phi_{max}) & \text{for m + n odd} \end{cases}$$

where $2\phi_{max} r_c$ is the total arc of the circle.

$$\text{for } t > t_2 \qquad \underline{m} = \begin{bmatrix} \sin\theta\cos\phi \\ \sin\theta\sin\phi \\ \cos\theta \end{bmatrix} \qquad \underline{p} = R \begin{bmatrix} \sin\theta\cos\phi \\ \sin\theta\sin\phi \\ \cos\theta \end{bmatrix} \qquad \begin{aligned} \theta &= \pi/2 - \psi \\ \psi &= \frac{v_e(t-t_2)}{R} \end{aligned}$$

Substitution in (2) results in:

$$\text{if } m = 0 \text{ then } a^*_{no} = 2nR^n P^o_n(\cos\theta) \sin\theta.\phi_{max}$$

$$\text{if } m \neq 0 \text{ then } a^*_{nm} = \frac{4}{m} \frac{(n-m)!}{(n+m)!} nR^n P^m_n(\cos\theta) \sin\theta \sin(m\phi_{max})$$

Again simplifications occur, when $\phi_{max} = \pi/2$, which is the case for

$$0 < t < t_1 \qquad \text{and} \qquad t_3 < t \leq t_4$$

Once these endocardium front activities are calculated, the a^*_{nm} need to be filtered in order to obtain the myocardium activity.
The resulting normalised potential can be written as:

$$\Phi = \frac{1}{r} \sum_{n=1}^{\infty} \sum_{m=o}^{n} \frac{1}{r^n} P_n^m(\cos \theta_r) a_{nm} \cos(m\phi_r) \qquad (3)$$

The coefficients a_{nm} are obtained by filtering a^*_{nm}. For simplicity digital filtering is performed.
As denoted before a distinction is made between the septum activity and the rest of the ventricle walls. Define that part of a^*_{nm}, that represents the septum activity by a^*_s and the rest by simply a^*. In the same way the subscripts L and R can be joined for the left and right ventricle respectively. The subscripts m and n are omitted now for clearness' sake. Choose a sample time $\Delta t(10^{-3}$ sec).
The filtering process is then represented by:

$$a(i) = \sum_{k=o}^{n_{RS}} a^*_{RS}(i-k) + \sum_{k=o}^{n_{LS}} a^*_{LS}(i-k) +$$

$$+ \sum_{k=o}^{n_R} a^*_R(i-k) + \sum_{k=o}^{n_L} a^*_L(i-k) \qquad \text{for } i-k > 0$$

where

$$a^*(i) = a^*_{nm} \qquad \text{for} \quad t = i\Delta t$$

and

$$n_L = \frac{d_L}{v_1 \Delta t} \qquad n_R = \frac{d_R}{v_1 \Delta t}$$

$$n_{LS} = \frac{d_{LS}}{v_1 \Delta t} \qquad n_{RS} = \frac{d_{RS}}{v_1 \Delta t}$$

Table 1 gives the values for the variables in the above formulas.

4. Relative importance of multipoles

The subscript n in formula 3 denotes the order of the multipole. It is interesting to know how much each multipole contributes to the potential. In view of the relative distances we compare the surface potentials for patients with the potential on a sphere with a radius, that equals two times the radius of the heart sphere and that is concentric with it.
The root mean square value of the potential on the surface of that sphere is given by:

$$\Phi_a = \sqrt{\frac{1}{4\pi(2R)^2} \iint_{\text{sphere}} \Phi^2 (2R)^2 \sin\theta \, d\theta d\phi}$$

Because of the orthogonality relationships for associated Legendre polynomials Φ_a becomes:

$$\Phi_a = \sqrt{\frac{1}{(2R)^2} \sum_{n=1}^{\infty} \sum_{m=o}^{n} \frac{1}{(2R)^{2n}} (a_{nm}^2 + b_{nm}^2) \frac{1}{2n+1} \frac{(n+m)!}{(n-m)!} \frac{1}{2 - \delta_m^o}}$$

For each n we find the contribution of the respective multipole to the mean square value of the potential on the sphere surface:

$$C_n^2 = \sum_{m=o}^{n} \frac{1}{(2R)^{2n+2}} a_{nm}^2 \frac{1}{2n+1} \frac{(n+m)!}{(n-m)!} \frac{1}{2 - \delta_m^o}$$

The roots of these values are plotted as a function of time in figure 5. Reflections on this plot lead us to the following remarks:

1) The dipole and quadrupole components located in the origin of the coordinate system are insufficient to describe the potential satisfactorily at a distance of two times the heart radius. Of course in reality the electrodes are often placed at a greater distance. For a time independent two-dimensional experiment Kempner and Grayzel (ref. 24) already noted the importance of the octapole in relation to the quadrupole.

2) For the septum activity the dipole component is strongly predominant. This is very encouraging, because Schubert (ref. 27) came to the same conclusion in his experimental research based on real data.
Some remarks about the mathematical background can be given. A homogeneous double layer with a circular boundary has only multipoles for odd n, when the expansion is made in the origin of the circle (see e.g. Burger ref. 31). The rings, which appear in the septum, can be supposed as a difference between two circular lamina with different radii. In that case the multipole expansion of the ring consists of the algebraic sum of the expansions of the circular lamina, which means, that the quadrupole and all even multipoles are missing. See figure 6a.
3) For the quadrupole component as a function of the time one can distinguish two peaks, which also agrees with the work of Schubert (27) and Taccardi (29).
Again some mathematical considerations are pertinent. The field due to a small double layer is given by:

$$\Phi(\underline{r}) = \pm C\, m(\underline{r}')\, d\Omega\, (\underline{r},\underline{r}')$$

where

C is a constant, depending on the medium.
$\underline{r}$ is the observation point
$\underline{r}'$ is the source point
m is the dipole strength per surface area
$d\Omega$ is the solid angle subtended by the small double layer at $\underline{r}$
The sign depends on the side from which the layer is observed.

When we deal with a homogeneous double layer, only the rim contributes to the outside field because all solid angles, in which the rim is not involved, are subtended to opposite double layer segments with equal positive and negative contributions.
The double layer rings, which appear in the outside walls of the ventricles, can then be represented by two circular lamina as figure 6b shows. These can be simulated very well by single dipoles. The result is then a pair of opposite neighbouring dipoles, which cause a strong quadrupole.
4) The quadrupole to dipole ratio, which is shown in figure 5 agrees with the experimental curves of Hlavin and Plonsey (ref. 26) as far as the high ending of the curve is concerned. This can be explained by the strong eccentricity of dipole activity during the end of the QRS-complex.

5) The validity of the foregoing remarks is restricted by the fact, that the multipole expansion is made with respect to the origin of the coordinate system. In sections 8 and 9 we will comment on this restriction.

5. Comparison with a multiple dipole model

Now we will evaluate to what degree the string model can be approximated by a small number of dipoles with fixed origin and direction, but varying in amplitude as a function of time.

Figure 7a shows an example, where only six dipoles are used. All dipoles except for dipoles V and VI are situated in the x-z-plane. Because of the symmpetry with respect to the x-z-plane the intensities of dipoles V and VI will show the same function of time. Thus the potential is depending on five functions of the time. In the multipole expansion the dipole and quadrupole components together were defined also by five time functions a_{nm}. In that sense the six dipole model can be compared with the string model, when only the dipole and quadrupole components are considered. Each dipole stands for the action of a special part of the heart in a special direction:

dipole I : total septal activity

dipole II : all dipole activity directed to the positive x-axis.

dipole III : dipole activity of left ventricle directed to the positive z-axis.

dipole IV : dipole activity of right ventricle directed to the negative z-axis.

dipole V : all dipole activity in the direction of the positive y-axis

dipole VI : all dipole activity in the direction of the negative y-axis.

The positions $\underline{p}_i$ of the dipoles are chosen to be the points of gravity of the respective double layers. Because the points of gravity change as a function of time, the average weighted with the dipole moment position, is chosen.

A better criterion for $\underline{p}_i$ would be the resemblance with the string model potential in some observation points. In that case however the origins of the dipoles change with the positions of the observation points, which we want to avoid.

Table 2 shows the spherical coordinates of $\underline{p}_i$ and the directions of the dipoles.

dipole number	I	II	III	IV	V	VI
$\lvert \underline{p}_i \rvert$ in cm.	1.06	4.80	4.32	4.32	5.96	5.96
θ_p in radians	$\pi/2$	1.32	0.24	2.90	1.25	1.25
ϕ_p in radians	0	0	0	0	1.33	- 1.33
direction of $\underline{m}_i$	- z	+ x	+ z	- z	+ y	- y

table 2.

Figure 7b shows the several dipole intensity functions. Referring to formula's 1 and 2 the potential due to the six dipole model can be evaluated in a multipole expansion, where

$$a_{nm} = \sum_{i=I}^{VI} (2-\delta_m^o) \frac{(n-m)!}{(n+m)!} |\underline{p}_i|^{n-1} \underline{m}_i^T \cdot \left\{ {}_nP_n^m(\cos\theta_{pi}) \begin{bmatrix} \sin\theta_{pi}\cos\phi_{pi} \\ \sin\theta_{pi}\sin\phi_{pi} \\ \cos\theta_{pi} \end{bmatrix} \cos m\phi_{pi} \right.$$

$$+ \frac{\partial P_n^m(\cos\theta_{pi})}{\partial\theta_{pi}} \begin{bmatrix} \cos\theta_{pi}\cos\phi_{pi} \\ \cos\theta_{pi}\sin\phi_{pi} \\ -\sin\theta_{pi} \end{bmatrix} \cos m\phi_{pi} +$$

$$\left. + P_n^m(\cos\theta_{pi}) \begin{bmatrix} -\sin\phi_{pi}/\sin\theta_{pi} \\ \cos\phi_{pi}/\sin\theta_{pi} \\ 0 \end{bmatrix} \cdot -m\sin\phi_{pi} \right\}$$

Although it is easy to evaluate the potential due to several dipoles directly, above multipole expansion is used, because it is suitable for comparison with the string model. We have noticed, that a multipole expansion facilitates the evaluation of the means square value of the potential over the surface of a sphere. Figure 8a shows the multipole components of this Φ_{a6D} as a function of time for the six dipole model and a sphere of radius 2R. The first five multipole components are taken into account.

The relatively high values of multipoles 4 and 5 attrack attention; this is accentuated by figure 8b. Here the mean square values of the difference in potential between the string model and the six dipole model are shown for the same sphere and for each multipole:

$$\sqrt{\sum_{m=o}^{n} \frac{1}{(2R)^{2n+2}} \left(a_{nmS} - a_{nm6D}\right)^2 \frac{1}{2n+1} \frac{(n+m)!}{(n-m)!} \frac{1}{2 - \delta_m^o}}$$

where S denotes the string model and 6D the six dipole model. The reason for these high values of multipoles 4 and 5 has to be sought in the lumping of the double layer in separated dipoles. A plane parallel to the septum contains three dipoles. The positions and directions of these dipoles II, V and VI promote the influence of the fourth harmonic in ϕ. It is inherent in the multipole expansion, that cos 4ϕ appears only in multipoles number 4 and higher. Consequently it is not amazing, that the coefficients a_{44} and a_{54} of the six dipole model are respectively 14 and 11 times those of the string model.

When we tried to limit these higher order multipoles by a smaller number of dipoles, for example by omitting dipoles V and VI, which cancel each other in the dipole component, it was found, that almost no resemblance was left in the quadrupole component.

The only remedy seems to be to use many more dipoles. The six dipole model under discussion is only suitable for taking care of the dipole and quadrupole resemblance. The higher order components show only resemblance in magnitude, but not qualitatively as is seen, when one compares figure 5 and figure 8.

More conclusions and comparisons between the several models will be made on the basis of the potential on a surface, being the boundary of the conducting medium.

6. The effect of a spherical boundary

The formula used until now for the potential in an conducting infinite medium:

$$\Phi = \sum_{n=1}^{\infty} \sum_{m=o}^{n} \frac{1}{r^{n+1}} P_n^m(\cos \theta_r)\, a_{nm} \cos (m\phi_r)$$

is in fact the particular solution Φ_p of $\Delta\Phi = f$, (Poisson's equation) where f is the forcing function of the dipole layers. If the conducting medium is bounded, a homogeneous solution Φ_h has to be added so that on the boundary:

$$\left[\nabla_{\underline{r}}(\Phi_p + \Phi_h)\right]^T \underline{n} = 0$$

where $\underline{n}$ is the normal on the boundary surface.
Because of the symmetry with respect to the x-z-plane:

$$\Phi_h = \sum_{n=1}^{\infty} \sum_{m=o}^{n} \left(\frac{\beta_{nm}}{r^{n+1}} + \alpha_{nm} r^n\right) P_n^m(\cos \theta_r)\cos(m\phi r)$$

If we choose a concentric sphere as the boundary, the homogeneous solution within this sphere has to be finite for r = 0. This implies, that all β_{nm} are zero. The α_{nm} are found in the boundary condition:

$$\frac{\partial \Phi_h}{\partial r} = -\frac{\partial \Phi_p}{\partial r} \quad \longrightarrow \quad \frac{n+1}{R_b^{n+2}} a_{nm} = n R_b^{n-1} \alpha_{nm}$$

where R_b is the radius of the sphere.
This implies, that the potential on the surface is given by:

$$\Phi = \sum_{n=1}^{\infty} \sum_{m=o}^{n} \frac{1}{R_b^{n+1}} \frac{2n+1}{n} P_n^m(\cos \theta_r)\, a_{nm} \cos (m\phi_r)$$

We observe, that each a_{nm} has to be multiplied by $\frac{2n+1}{n}$ in order to find potentials on a spherical boundary. It implies, that high order multipoles are reduced in strength compared to lower order multipoles.

7. Deviations of the one-dipole, the dipole and quadrupole, and the six dipole model in comparison with the string model.

In this section we will compare several models with the string model. The criterion will be the surface potential differences on a spherical boundary. The root mean square values of the potential differences on a spherical boundary with radius R_b are as follows:

For the *one dipole model:*

$$\Phi_{aD} = \sqrt{\sum_{n=2}^{\infty} C_n^2}$$

where

$$C_n^2 = \frac{1}{(R_b)^{2n+2}} \frac{2n+1}{n^2} \sum_{m=o}^{n} a_{nmS}^2 \frac{(n+m)!}{(n-m)!} \frac{1}{(2-\delta_m^o)}$$

and subscript S denotes string model. (see section 4)

When the *dipole and quadrupole* components are used:

$$\Phi_{aD+Q} = \sqrt{\sum_{n=3}^{\infty} C_n^2}$$

The error of the *six dipole model* is given by:

$$\Phi_{a6D} = \sqrt{\sum_{n=1}^{\infty} \frac{1}{(R_b)^{2n+2}} \frac{2n+1}{n^2} \sum_{m=o}^{n} (a_{nmS} - a_{nm6D})^2 \frac{(n+m)!}{(n-m)!} \frac{1}{2-\delta_m^o}}$$

In order to compare these functions for several R_b, the relative error is defined by dividing these functions by the RMS of the potential of the string model:

$$\Phi_a = \sqrt{\sum_{n=1}^{\infty} C_n^2}$$

In these expressions the upper limit of the summations is infinite. In our computer programs only five multipoles were calculated. It is easy to see, that taking more multipoles into account will enlarge the relative errors of the one dipole model and the dipole and quadrupole model, because $C_n^2 > 0$. Because a_{nm6D} does not look like a_{nms} for higher values of n, it may be expected, that also for the six dipole model the error found here is a lower bound. The small values of a_{nms} for $n > 6$ ensure us, that only small deviations have to be expected. Figure 9 shows these relative errors of the different models for R_b = 2R, 3R and 4R where R is the radius of the heart sphere. In order to relate these curves to the averaged potential on the boundary, Φ_a is given too.
The following remarks can be made.

1) During the activity of the septum, i.e. $0 < t < 30$ (m sec), small errors are found for all models. This is due to the fact, that a dipole alone in the center of a flat double layer can simulate the field of that double layer quite accurately. In section 4 this phenomenon is mentioned already.
   Because of partial cancellation of double layers in the right and left part of the septum, the total activity Φ is relatively small in this interval.
2) For $30 < t < 50$ (m sec) the outside walls of the ventricles are active. As figure 4 shows, in this period the largest double layer exists in the form of rings. A high extent of eccentricity is reached and the directions of the dipoles in the double layers are widely different. Consequently the Φ_a is maximal, but the models fail. All relative errors of the models show a peak at about 40 m sec. The model, which uses a dipole and quadrupole term, can handle this situation most adequately.
3) In the interval $50 < t < 80$ (m sec) the errors are rather large due to the facts mentioned under 2.
   The lack of the quadrupole contribution is easy to recognize in the Φ_{aD}/Φ_a; Φ_{aD+Q}/Φ_a shows the absence of the third order multipole. (see also figure 5).
4) At the end of the QRS-complex (80-95 m sec) one can distinguish two rather flat double layers, wherein the dipoles are mainly directed along the z-axis. It was to be expected, that the six dipole model could simulate this accurately, but the errors are still disappointingly large. The origins of dipoles III and IV may not be optimal.

The errors during this period are in general large, but the total Φ_a diminishes rapidly.

5) On the whole the Φ_{a6D} and Φ_{aD+Q} are substantially better than Φ_{aD}. The Φ_{aD+Q} seems to result from a better simulation then the Φ_{a6D}, where both models are described by five time functions.

6) The errors Φ_{aD} and Φ_{aD+Q} are essentially greater then found in practice (ref. 27, 30). The reason will be the choice of the origin, where the expansion is made. Geselowitz (ref. 25) suggested a method for determining an optimal origin. He assumes, that multipoles of an order higher than the quadrupole are neglectible. In the optimal origin the quadrupole component is minimal. The formula he derived is:

$$\begin{bmatrix} x_o \\ y_o \\ z_o \end{bmatrix} = |\underline{p}|^{-4}(|\underline{p}|^2 I - \tfrac{1}{2}\underline{p}\,\underline{p}^T)\,Q\underline{p}$$

where $\underline{p}$ is the vector of dipole components and the matrix Q contains quadrupole coefficients. Application of this formula gives us the coordinates of the origin as a function of time. Because of the symmetry the y_o will always be zero. For the string model the result is shown in figure 10. As had to be expected the optimal origin moves in the interval $0 < t < 30$ (m sec) from the origin of the coordinate system along the positive x-axis. When the time proceeds from 30 to 40 m sec a strange loop occurs, which may be due to the neglection of multipoles of higher order then the quadrupole. Form 40 to 50 m sec the origin is rather stable. Afterwards the left ventricle activity seems to be predominant and consequently the origin moves along the positive z-axis. Because the last depolarisation takes place on the z-axis for z = 6 cm, the origin will be found there at the end of the depolarisation wave. Generally the tendency exixts, that the origin moves along the positive x-axis and the positive z-axis.

In ref. 27 Schubert gives an optimal trajectory of the origin calculated from real data. Some resemblance can be recognized. He also found, that the optimal origin is rather time independent during the periods 0-20 m sec and 80-100 m sec. During the time from 20 m sec until 30 m sec both pictures shows a course along a straight line. Schubert remarks, that in the periods 30-50 m sec and 60-70 m sec the method fails more or less because of the big quadrupole to dipole ratio, which is the same in our case. (see figure 5).

According to Durrer (ref. 21, 22, 23) the activation ends in the basical right ventricle and septum wall. The optimal origin at the end of the QRS-complex should be in that region then, in contrast with our model, where depolarisation ends in the left ventricle outside wall. In the following section more data and discussion on the optimal origin will be given.

8. Surface potentials

We have seen, that a spherical boundary was very easy to handle in calculations. We will use this boundary and evaluate the potentials in electrodes, equally distributed on the surface. Figure 11 shows a projection of the positions of the electrodes on the x-z-plane. The spherical coordinates are also given, where r is always Rb, the radius of the spherical boundary.
Electrodes positions 6, 7, 8 and 9 are chosen, in such a way, that the distances to the nearest electrodes on the axis are equal.
In the minus y half space one can define a same set of electrodes, but the symmetry of the heart will cause the same potentials in those electrodes.
The potentials in these nine electrodes are very representative for potentials on the whole surface, because errors, as defined in section 7, were calculated for these nine electrodes instead of integration over the whole surface and the resulting curves were the same as shown in figure 9.
The systematic placing of the electrodes provides simple formula's for the potentials, if the multipole coefficients are known.
In order to get an idea of the potential curves in the electrodes, figure 12 shows these potentials as a function of time for $R_b = 2R$ and $R_b = 4R$.
Allmost all potentials change only quantitatively as a function of R_b, except for potential-curves 1, 2 and 3.
Especially the potential of electrode 2 undergoes an essential change, if the radius of the sphere is doubled. This indicates a proximity effect with respect to the right ventricle. When the radius of the spherical boundary is large, the left ventricle dominates and consequently the potential is negative during the period from 40 till 100 m sec.
If on the otherhand the radius is small, then the field of the right ventricle is strong enough to cause a positive peak at 70 m sec, the moment, when the direction of the right ventricle double layer is directed towards the minus z-axis.
From the potential curves in figure 12 it is easy to see, that a dipole in the origin of the coordinate system is a bad model. Such a model provides signals in pairs of electrodes like 1 and 2 or 3 and 4, which would qualitatively show p_z and p_x respectively. These dipole components are drawn as dotted lines in the concerning plots. Because p_y is zero, electrode 4 would not even show any potential curve at all for a one dipole model. Although this sounds unfavourable for the one dipole model, with the aid of the intrinsic components it can be shown (section 9), that a better origin for that one dipole results in completely opposite conclusions.

Before determining these intrinsic components a last remark about figure 12 has to be made. The potential curves look like those measured on persons. This fact is very promising. More conclusions, however, can not be drawn in this stage of the research.
In the introduction it is already stressed, that the string model of the depolarisation wave fails in many details but that it shares the field properties with reality. Furthermore the spherical boundary is a very primitive representation of the human body.

9. Intrinsic components.

The nine electrode potentials of figure 11 span a timespace with dimension equal to or less than nine. The so called intrinsic components form an orthogonal basis for this space in such a way, that these respective canonical signals possess a diminishing importance. The factor analysis, used for this purpose, is described in many articles e.g. ref. 9, 10, 11 where it is adapted to this field of research. In a nutshell the procedure is as follows:

Using the nine electrode signals s_i a correlation matrix H can be formed where

$$|H_{ij}| = \int_0^{100\ \text{m sec}} s_i s_j dt$$

H can be written in a Jordan canonical form:

$$H = E\ \Lambda\ E^T$$

Λ - diagonal matrix containing eigenvalues of H in the order of diminishing magnitude

E - Matrix, whose columns are the corresponding eigenvectors.

The relation between the intrinsic components u_j and the electrode signals s_i is given by:

$$\underline{u} = E^T \underline{s} \qquad \text{and} \qquad \underline{s} = E\underline{u}$$

Furthermore

$$\int_0^{100\ \text{m sec}} u_i u_j dt = 0 \quad (i \neq j) \qquad \text{and} \qquad \int_0^{100\ \text{m sec}} u_i^2 dt = \lambda_i$$

which means, that the eigenvalues λ_i equal the energy of the corresponding intrinsic component.

Figure 13 shows the intrinsic components for three values of R_b. Comparison of these u_i with intrinsic components from real measurements (9, 10, 11) indicates, that there is a strong resemblance.

The relative importance of the different intrinsic components can be defined very easily using the eigenvalues λ_i. Suppose, that we want to simulate the signals s_i by s^*_{ip}, which is a linear combination of the p largest intrinsic components. Then $\underline{s}_p$ can be written as:

$$\underline{s}^*_p = E\underline{u}^*_p \qquad \text{because } \underline{s} = E\underline{u}$$

where $\underline{u}^*_p$ contains p elements of $\underline{u}$ and for the rest zero elements. The relative error can be defined by:

$$\sqrt{\frac{\int(\underline{s}-\underline{s}^*_p)^T(\underline{s}-\underline{s}^*_p)dt}{\int\underline{s}^T\underline{s}dt}} = \sqrt{\frac{\int(\underline{u}-\underline{u}^*_p)^TE^TE(\underline{u}-\underline{u}^*_p)dt}{\int\underline{u}^TE^TE\underline{u}dt}} = \sqrt{\frac{\sum_{i=p+1}^{9}\lambda_i}{\sum_{i=1}^{9}\lambda_i}}$$

These values and the functions

$$\frac{\lambda_j}{\sum_{i=1}^{9}\lambda_i}$$

are given in figure 13. It was found, that, within the accuracy of the computer (13 significant decimal digits in the mantissa), the dimension of the time space was eight instead of nine.
For all $R_b > 2R$ the first four intrinsic components define more then 96% of the total signals according to above criterion.
We would like to have an idea about the error as a function of time, which causes us to omit the integrals in above criterion. Then we cannot use the λ_i any longer, but the criterion is the same as we used for the other models:

$$\frac{\Phi_{up}}{\Phi_a} = \frac{\sqrt{(\underline{s}-\underline{s}^*_p)^T(\underline{s}-\underline{s}^*_p)}}{\sqrt{\underline{s}^T\underline{s}}}$$

These functions for different p and R_b are given in figure 14. The behaviour of these curves is remarkable for two reasons. The errors for a fixed number of time functions is much less then the errors of the models used untill now with that same number of time functions, especially in the interval from 40 m sec till the end. In contrast with the earlier models, however, the error during the septum activity is rather large. An explanation for this last phenomenon can be found, if we compare the intrinsic components with the dipole components. The intrinsic components U_1 and U_2 are highly correlated with the two dipole components p_x and p_z. Figure 15 shows two sets of three curves which are almost equal. One set is composed of the potential difference $S_1 - S_2$, the contribution to this potential difference of p_z and the contribution of U_1 and U_2. The other set shows the same for $S_3 - S_5$, p_x and U_1, U_2 respectively.

The resemblance of the curves implies, that on a distance $R_b = 4R$ the intrinsic components U_1 and U_2 can be obtained by rotation from the dipole components p_x and p_z with a small error. This rotation was necessary because in the time domain the p_x and p_z are generally not orthogonal. This is illustrated in figure 15b. It means, that choosing an optimal origin for the one dipole model is sufficient to obtain an error on a sphere of 4R, which is about 10% during the activity of the ventricle outside walls, as figure 14 shows. The optimal origin is somewhere in the quadrant $x > 0$ and $z > 0$. This can be seen using figure 16, which shows the image space with respect to the intrinsic components U_1 and U_2. All electrode potentials can be described by:

$$s_i = e_{1i}u_1 + e_{2i}u_2 + \ldots$$

The values e_{1i} and e_{2i} are the coordinates along the two axes of figure 16. The dotted lines denote the directions of p_x and p_z in this image space. Like in figure 15 these axes are found by a rotation over an angle α. Indeed the axes x^1 and z^1 are almost parallel to the lines of connection between the

images of electrodepairs 1-2 and 3-5. With the aid of these lines it is obvious, that the image of electrode 1 is built up by a small negative amount of p_x and a positive amount of p_z. This implies, that in the real space the position of the p_x will be in the positive x half space. Because of the small amount of negative p_z in the electrode signals 3 and 5, the origin of the p_z will be in the positive z half space. Theoretically it is not necessary now, that the origins of the p_x and p_z are the same. So it is possible, that we deal with the situation, that the two intrinsic components under discussion form such a good model because they simulate two separate dipoles. More research should be done on this aspect.

Nevertheless the eccentric position of the p_z is disadvantageous during sepseptum activity, which explains the larger error in this interval as figure 14 shows.

The conclusion may be drawn, that a carefully chosen origin for the dipole (or origins for 2 dipoles p_x and p_z) improves the simulation drastically.

10. Conclusions and future developments

A new mathematical model of the depolarisation wave is described, which is still primitive, but improvements can easily be made. Using this model it will be simple to simulate surface potentials in a mathematical model of the human body, where also the intracavitary blood mass and the lungs are incorporated.

In the present research the string model was used to test the other models. When the string model has been improved, it can be used for the inverse problem too, where the condition of the heart is determined from the electrode signals.

The agreement of the string model with reality lies espeically in the field properties. In ref. 28 Hlavin and Plonsey mention two main conditions, which cause a distributed source to behave like a dipole:

1) The observation point should be at a distance from the source, which is at least two times the extent of the source.
2) The sources can be approximated by a uniform double layer with a short rim.

In reality and in the string model the first condition is fairly satisfied. The second condition, however, contradicts with reality, where more active, separated layers exists, which have no short rims at all. The string model shares this last property with reality. These multiple layers cause the larger influence of higher order poles.

If the double layer has a circular rim the simulation by a single dipole is best as is seen for the septum. If the layer is strongly curved, however, then it is questionable how many dipoles can simulate the field in an appropriate way. The extreme of a curved plane is the closed ring with radial direction of the dipole layer, which can be found in the string model at about 30 m sec. In reality these rings exist too, be it not in such a pronounced way as in the string model.

Many others (ref. 2, 3, 4, 5, 6, 7, 8, 9) have considered the simulation of double layers by dipoles. In this article however, the influence of time is taken into account. It is rather simple to constitute a number of dipoles for simulation at a certain time, but the problem becomes more complex if fixed dipoles have to represent changing double layers.

The fact, that we introduced changing double layers with multiple rims, gives us a deeper insight into the validity of the one dipole model compared with the conclusions Frank made (ref. 32).

He found, that the one dipole was a good representation of a double layer with a circular rim; but this is a too simple representation of the depolarisation wave, Another conclusion he arrives, viz. that the importance of eccentricity effects are much more pronounced than the differences between dipole and double layer, is confirmed here. Indeed, the relatively unexplored effects of variable eccentricity during heart beat are still of great importance.

The capacity of the one dipole model to represent electrode potentials is confirmed, without the influence of inhomogeneties in the body. The potentials, however, are very sensitive to the origin of that one dipole. This fact has been recognised in literature many times. Some physical background concerning that optimal origin has been given. In section 9 a fixed origin was found with the aid of the intrinsic components, while in section 8 an optimal origin as a time function was determined. In the last case four time functions were used because of the symmetry of the heart. In this light it is remarkable, that only four predominant intrinsic components were distinguishable.

The multiple dipole model used is hardly better than the one dipole model. No research however has been done to optimize the origins and directions of the dipoles. We expect, however, that many fixed dipoles will be necessary to obtain a clearly better result than the one dipole model if we maintain the restriction, that the origins of the dipoles are in the region of heart segments which they have to represent.
As far as the multipole representation is concerned, it can be said, that the string model provides us with dipole and quadrupole components, which have much in common with those components measured in the practical situation. Furthermore it gives us an idea of the importance of the higher order multipoles, when the expansion is made with respect to the center of both ventricles.

Although we are aware of the fact, that the string model fails to represent the depolarisation wave exactly, we feel, that a model, which can not simulate the string model satisfactorily, will not be able at all to represent the more complex practical depolarisation wave.

Acknowledgement.

The author wishes to thank Professor Dr.Ir. P. Eykhoff, Ir. J. Blom, Ir. A.v.d. Boom and Ir. C.v.d. Brekel for reading the manuscript and offering suggestions and Miss. E. Sanders and Mr. v.d. Akker for the typing and the drawings.

Literature

1 D.B. Geselowitz, "Multipole representation for an equivalent cardiac generator", *Proc. IRE*, vol. 48, Jan. 1960, pp 75-79.

2 R. Bellman, C. Collier, H. Kagiwada, R. Kalaba and R. Selvester, "Estimation of heart parameters using skin potential measurements", *Comm. of the ACM*, vol. 7, No. 11, Nov. 1964, pp 666-668.

3 R.H. Selvester, C.R. Collier, R.B. Pearson, "Analog computer model of the vectorcardiogram", *Circulation*, vol. 31, Jan. 1965, pp 45-53.

4 M.S. Lynn, A.C.L. Barnard, J.H. Holt and L.T. Sheffield, "A proposed method for the inverse problem in electrocardiology", *Biophysical Journal*, vol. 7, 1967, pp 925-945.

5 C.L. Rogers and T.C. Pilkington, "Free-moment current dipoles in inverse electrocardiography", *IEEE Trans. Bio-Med. Eng.*, vol. BME-15, No. 4, Oct. 1968, pp 312-323.

6 J.H. Holt, A.C.L. Barnard, M.S. Lynn and P. Svendsen, "A study of the human heart as a multiple dipole electrical source", *Circulation*, vol. 40, Nov. 1969, pp 687-718.

7 R.M. Rosenberg, C.H. Chao and J. Abbott, "A new mathematical model of electrical cardiac activity", *Mathematics Biosciences*, vol. 14, 1972, pp 367-394.

8 D.A. Brody and J.A. Hight, "Test of an inverse electrocardiographic solution based on accurately determined model data", *IEEE Trans. Bio-Med. Eng.*, vol. BME-19, No. 3, May 1972, pp 221-228.

9 A.A. Damen and H.A. Piceni, "The multiple dipole model of the ventricular depolarisation", *TH-Report* 71-E-25, Oct. 1971, University of Technology, Eindhoven Netherlands.

10 A.M. Scher, A.C. Young and W.M. Meredith, "Factor analysis of the electrocardiogram", *Circulation Research*, vol. 8, May 1960, pp 519-526.

11 T.Y. Young and W.M. Huggins, "The intrinsic component theory of electrocardiography", *IRE Trans. Bio-Med. Electron.*, vol. 9, Oct. 1962, pp 214-221.

12 L.G. Horan, N.C. Flowers and D.A. Brody, "Principal factor waveforms of the thoracic QRS complex", *Circulation Research*, vol. 15, Aug. 1964, pp 131-145.

13 R. Plonsey and D.B. Heppner, "Considerations of quasi-stationarity in electrophysiological systems", *Bull. of Math. Biophysics*, vol. 29, 1967, pp 657-664.

14 D.A. Brody, "A theoretical analysis of intracavitary blood mass influence on the heart lead relationship. *Circulation Research*, vol. 4, 1956, pp 731-738.

15 D.B. Geselowitz and H. Ishiwatari, "A theoretic study of the effect of the intracavitary blood mass on the dipolarity of an equivalent heart generator", *Proc. Long Island Jewish Hosp. Symposium vectorcardiography* 1965, North-Holland Publishing Co.

16 T.C. Pilkington, R.C. Barr and C.L. Rogers", Effect of conductivity interfaces", *Bull. of Math. Biophysics*, vol. 29, 1967, pp 705-709.

17 S. Rush, "An inhomogeneous anisotropic model of the human torso for electrocardiographic studies", *Med. & Biol. Eng.*, vol. 9, 1971, pp 201-211.

18 R.M. Arthur and D.B. Geselowitz, "Effect of inhomogeities on the apparent location and magnitude of a cardiac current dipole source", *IEEE Trans. Bio-Med. Eng.*, vol. BME-17, No. 2, April 1970, pp 141-146.

19 A.M. Scher and A.C. Young, "The pathway of ventricular depolarisation in the dog", *Circulation Research*, vol. 4, July 1956, pp 461-469.

20 A.M. Scher, "Excitation of the heart", in *Handbook of Physiology*, Circulation vol. 1, American Physiological Society, Washington D.C. 1962.

21 D. Durrer, "Electrical aspects of human cardiac activity: a clinical - physiological approach to excitation and stimulation", *Cardiovasc. Res.*, vol. 2, 1968, pp 1-18.

22 D. Durrer, R.Th. van Dam, G.E. Freud, F.L. Meijler and J.P. Roos, "Excitation of the human heart", in *Electrical Activity of the Heart*, chapter 5, ed. by G.W. Manning and S.P. Ahuja, publ. C.C. Thomas, Springfield, Illinois, U.S.A.

23 D. Durrer, R.Th. van Dam, G.E. Freud, M.J. Janse, F.L. Meijler and R.C. Arzbaecher, "Total excitation of the isolated human heart", *Circulation*, vol. 41, June 1970, pp 899-912.

24 K.M. Kempner and J. Grayzel, "Single dipole, multiple dipole and dipole-quadrupole models of the double-layer in a circular lamina", *J. Electrocardiology*, vol. 3, No. 2, 1970, pp 95-110.

25 D.B. Gesolowitz, "Two theorems concerning the quadrupole applicable to electrocardiography", *IEEE Trans. Bio-Med. Eng.*, vol. BME-12, No. 3 and 4, July/Oct. 1965, pp 164-168.

26 D.A. Brody, J.C. Bradshaw and J.W. Evans, "A theoretical basis for determining heart lead relationships of the equivalent cardiac multipole", *IRE Trans. on Bio-Med. Electron.*, April 1961, pp 139-143.

27 R.W. Schubert, "An experimental study of the multipole series that represents the human electrocardiogram", *IEEE Trans. Bio-Med. Engr.*, vol. BME-15, No. 4, Oct. 1968, pp 303-312.

28 J.M. Hlavin and R. Plonsey, "An experimental determination of a multipole representation of a turtle heart", *IEEE Trans. Bio-Med. Electron.*, vol. 10, No. 3, July 1963, pp 98-105.

29 B. Taccardi, "Distribution of heart potentials on the thoracic surface of normal human subjects", *Circulation Research*, vol. 12, April 1963, pp 341-352.

30 E. Frank, "Determination of the electrical center of ventricular depolarisation in the human heart", *Am. Heart. J.*, vol 49, 1955, pp 670-692.

31 H.C. Burger, "Heart and vector", *Philips Technical Library*, 1968, Eindhoven, Netherlands.

32 E. Frank, "A comparative analysis of the eccentric double-layer representation of the human heart", *Am. Heart. J.* vol. 46, 1953, pp 364-378.

General notations

$\underline{a}$ vector

$a = |\underline{a}|$ = length of vector $\underline{a}$

$\underline{a}^T$ = $\underline{a}$ transposed

$\nabla_{\underline{a}}$ = gradient with respect to $\underline{a}$

< > brackets used, when almost the same formula holds for several variables between these brackets.

[ ] vector brackets.

$\frac{\partial a}{\partial b}$ specific derivative

List of important variables

c_n^2 = contribution of the n-th multipole to the square value of the potential on the spherical surface

d = local thickness of the heart wall

dl = small integration part of a string

δ_m^o = Kronecker delta

l = distance between base and origin

$\underline{m}$ = dipole intensity per unit length in each direction

$\underline{m}_I$, $\underline{m}_{II}$ etc = dipole strength of corresponding fixed dipole

m = order of harmonic

n = order of multipole

nL, nR, nLS, nRS = duration of impulsresponse in number of samples for the different heart parts.

P_n^m = associated Legendre function of the first kind

$\underline{p}$ = position of a small dipole string

$\underline{p}_I$, $\underline{p}_{II}$ etc = position of fixed dipoles

$\underline{r}$ = position of the observation point

R = radius of the heart sphere

R_b = radius of the boundary sphere

r_c = radius of the depolarisation front in the septum

σ = specific conductivity

t = time in m sec

Δt = small time interval or sample time

t_1 = beginning of the QRS-complex

t_2 = ending of the septum endocardium activity

t_3 = the time at which the depolarisation front in the endocardium of the ventricles closes into circles.

t_4 = ending of the depolarisation front in the endocardium

T = duration of impuls response

v_e = the propagation speeed of the depolarisation through the endocardium $\approx$ velocity in Purkinje fibers.

v_1 = the propagation speed through the myocardium

Ψ = angle in x-z plane

Φ = normalized potential

V = field potential

θ, ϕ = spherical coordinates

ϕ_{max} denotes the end of a string

x, y, z = rectangular coordinates

$*$ denotes, that the "filtering action" is not yet performed.

Table 1 values of important constants.

$|\underline{m}| = 1 \ \frac{Am}{m} = 1A$

$R = .06$ m

$l = .03$ m

$v_e = 2 \ ^{m}/sec$

$v_1 = 1 \ ^{m}/sec$

$d_R = .0054$ m

$d_L = .018$ m

$d_{RS} = .0027$ m

$d_{LS} = .009$ m

$\Delta t = 1$ m sec.

$t_1 = 15$ m sec.

$t_2 = 30$ m sec.

$t_3 = 61$ m sec.

$t_4 = 77$ m sec.

$nL = 18$

$nR = 5$

$nLS = 9$

$nRS = 3$

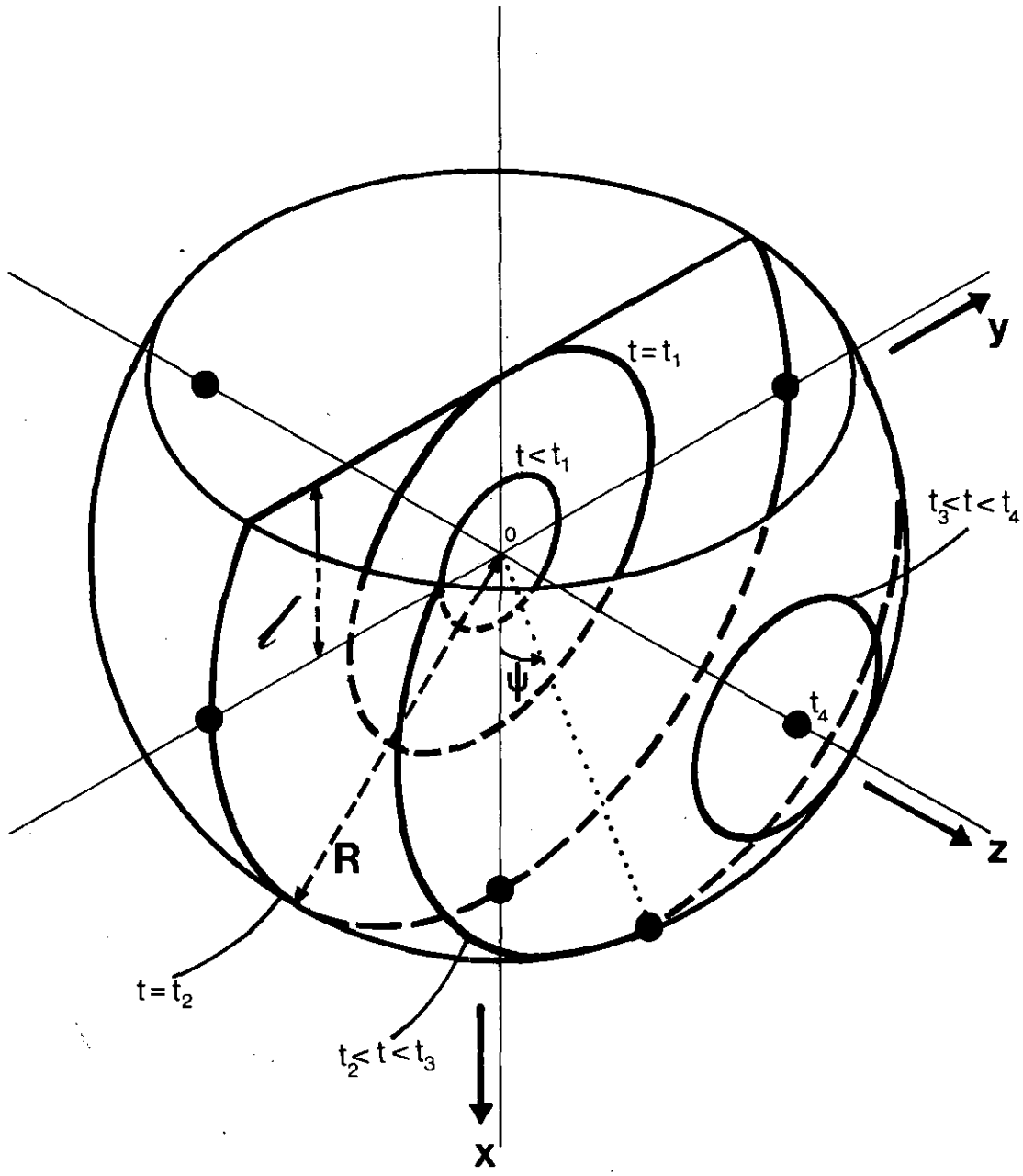

figure 1

Representation of the heart in the string model.

The walls are infinitesimally thin.

The heart sphere (radius R) is truncated by the base, a plane perpendicular to the x-axis in x = -1.

The septum is situated in the x-y-plane

The angle Ψ (in the x-z-plane) denotes the current position of the depolarisation front in the endocardium.

The left ventricle is on the positive z side.

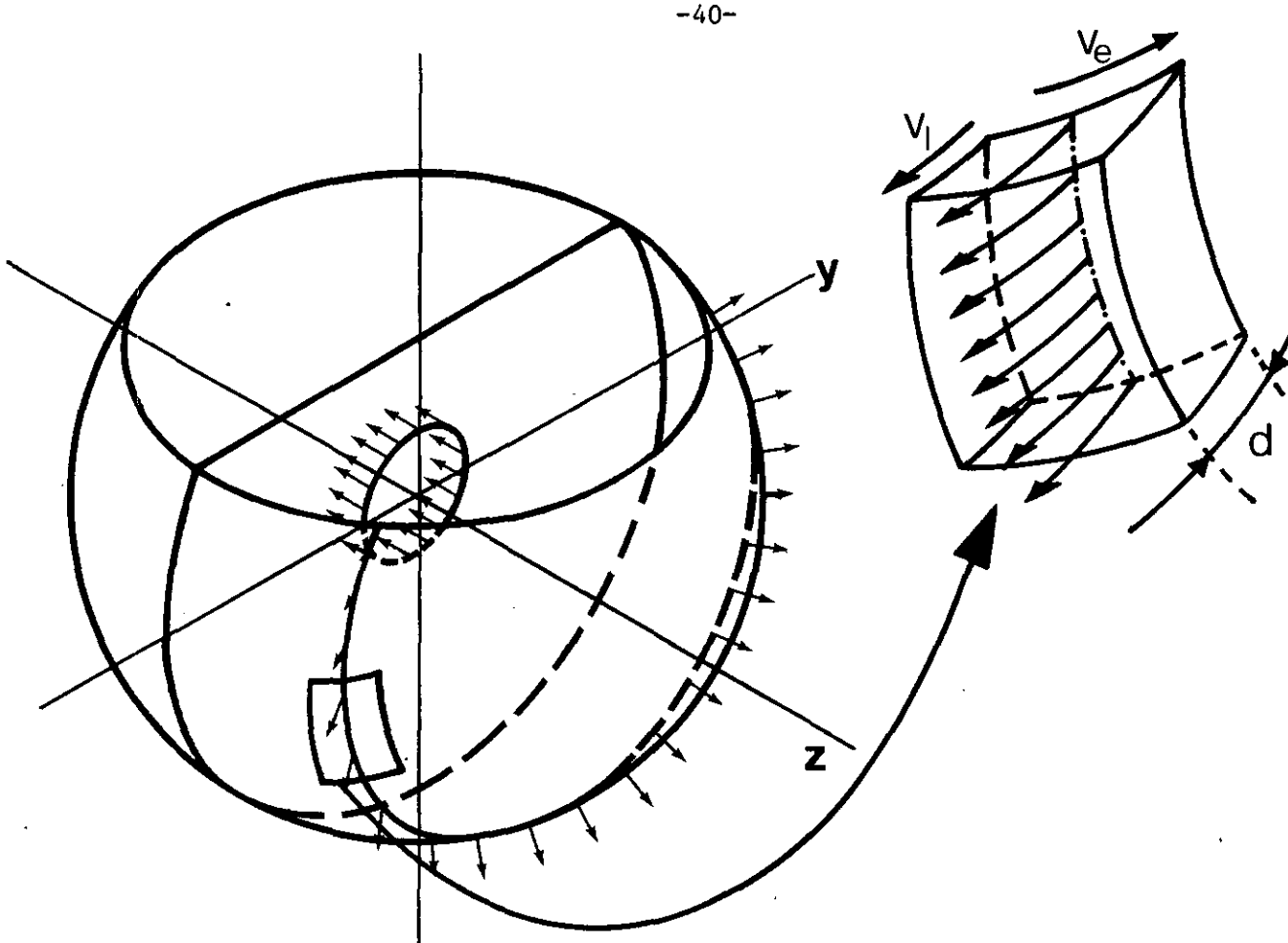

figure 2

Schematic of the direction of the depolarisation wave. The direction of its tangential and radial velocities (V_e and V_l respectively) are indicated.

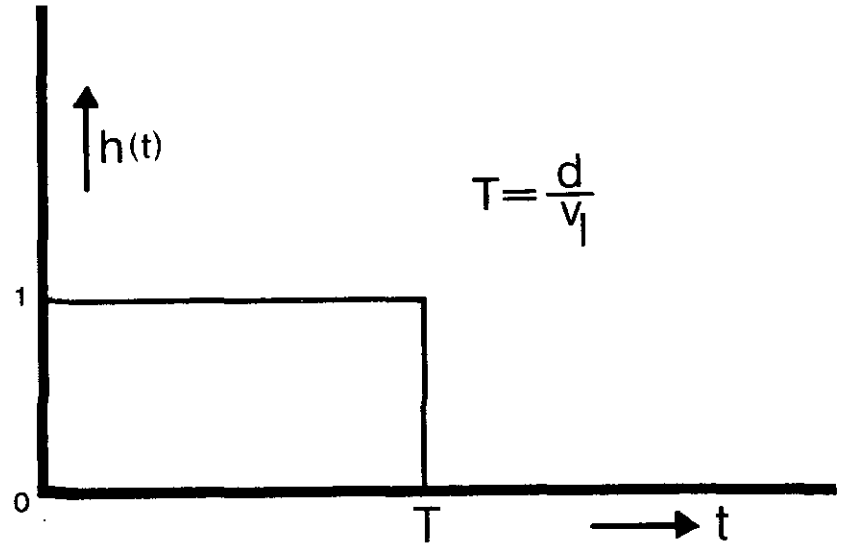

figure 3

The impulse response, which represents the depolarisation wave through the myocardium.

The dipole string, triggered in the endocardium, is maintained by the myocardium during a time, proportional to the local thickness of the myocardiu

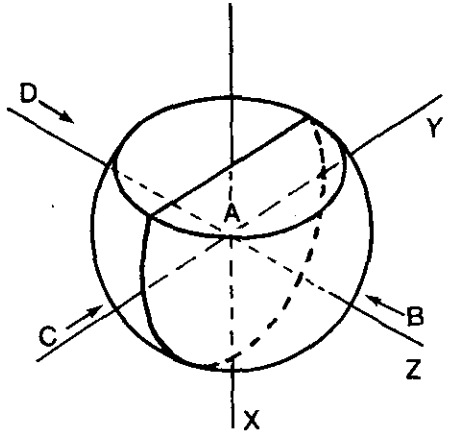

figure 4

The double layer (shaded areas) at several moments.

View A: The septum seen from the positive z-axis. (left ventricle is omitted)

View B: The left ventricle seen from the positive z-axis.

View C: Anterior view from the negative y-axis.

View D: The right ventricle seen from the negative z-axis.

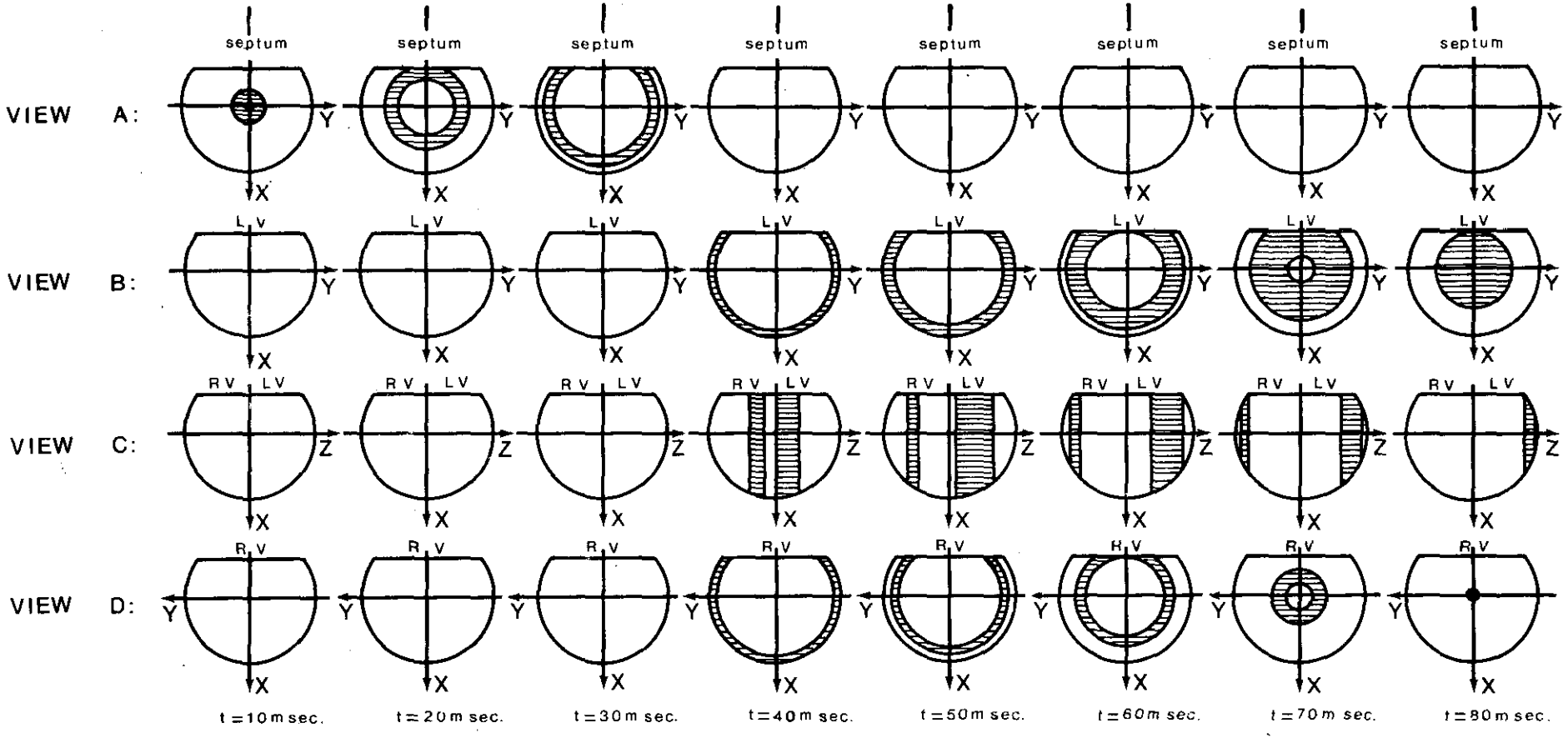

FIGURE 4

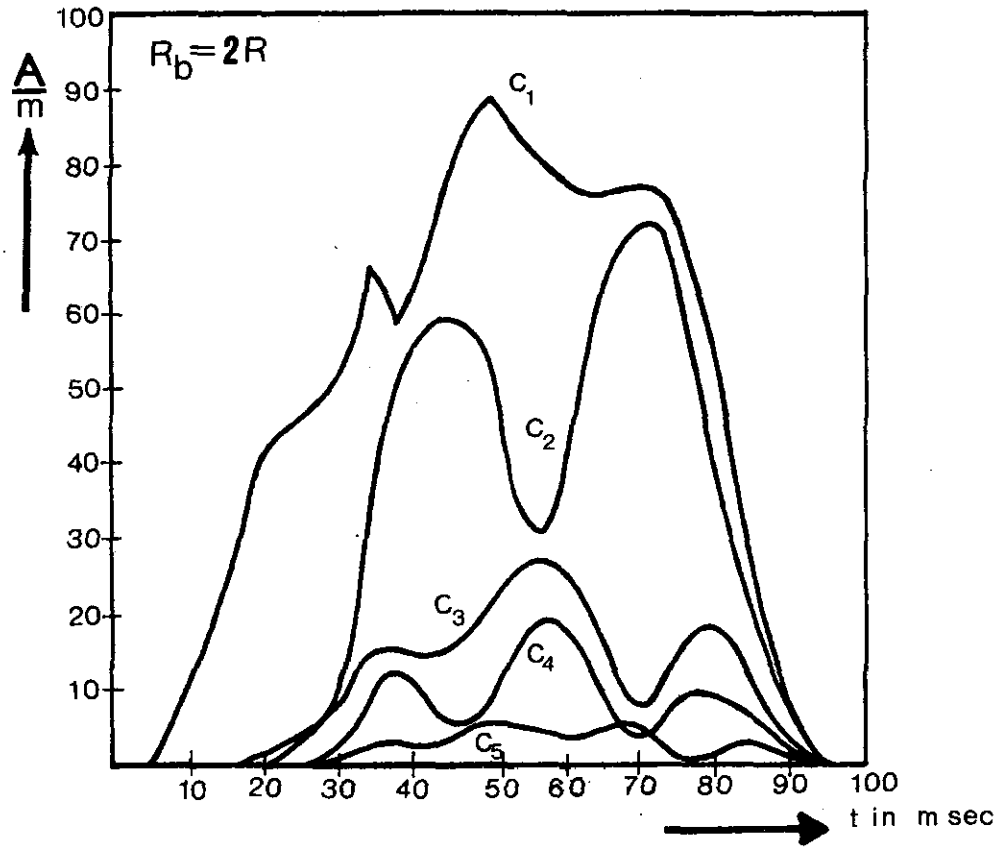

Different contributions C_n of the multipoles to the RMS of the potential on a sphere with radius 2R. (see section 4).

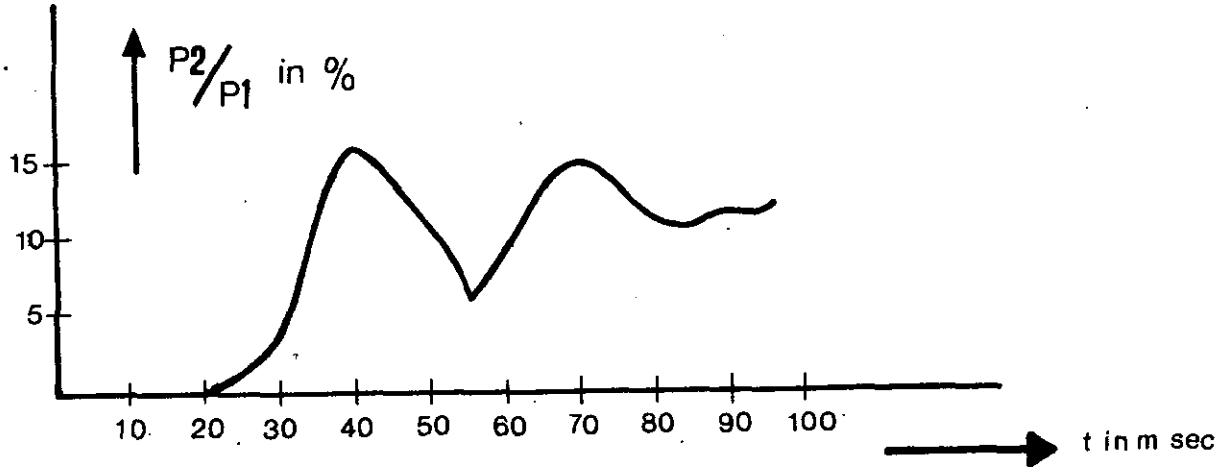

The quadripole to dipole ratio is also given.

The strengths of these multipoles are determined according to the definition, given by Geselowitz (ref. 25).

FIGURE 5

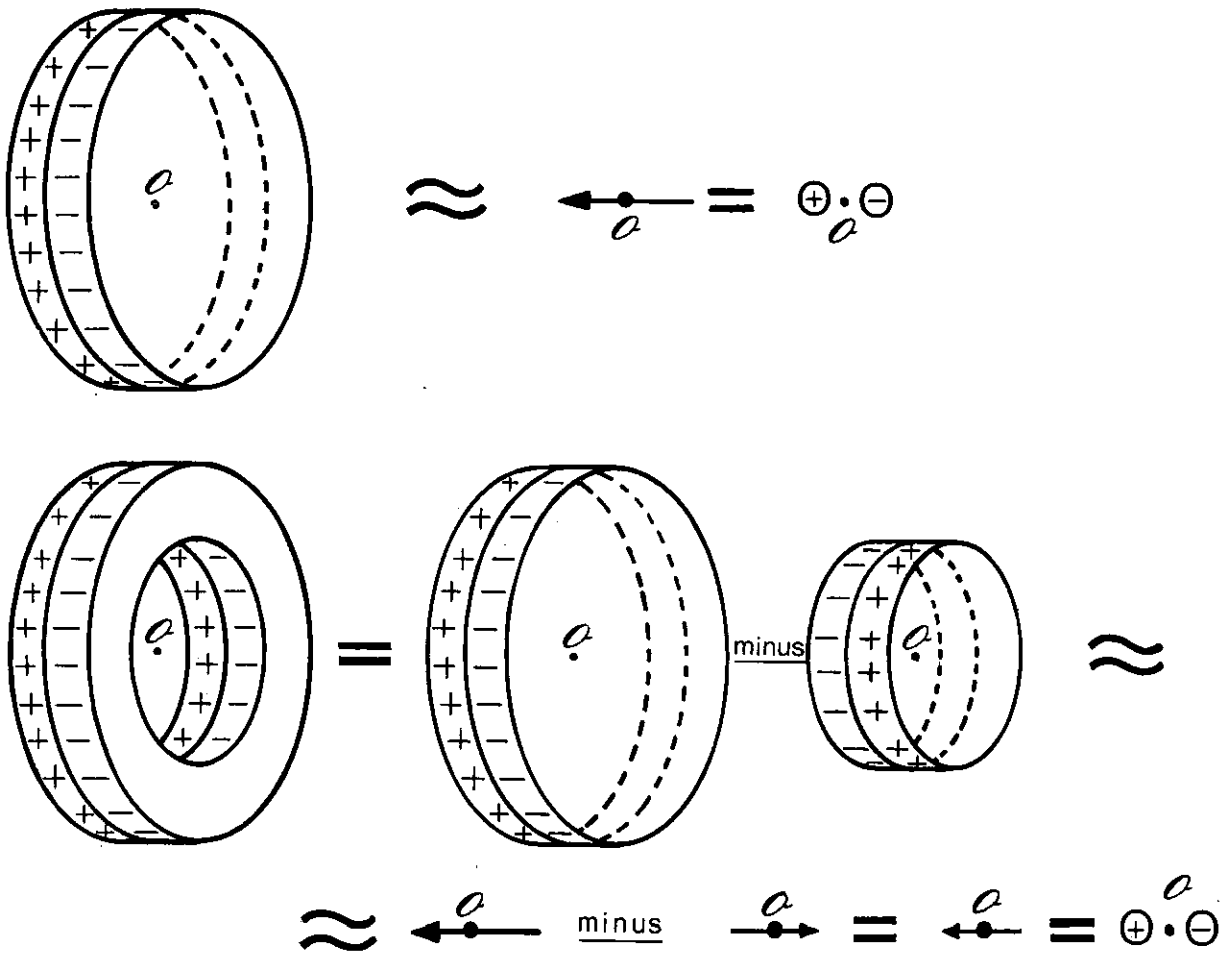

figure 6a

Illustration of the way the septum activation is simulated by a dipole.

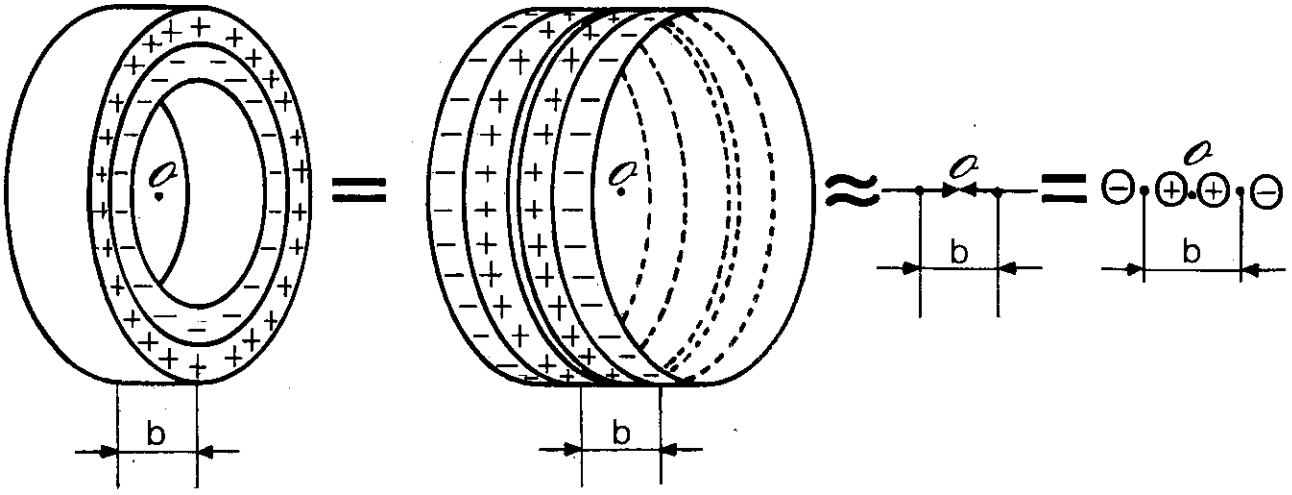

figure 6b

A ring with a homogeneous, radially directed dipole layer possesses no resulting dipole component, but a strong quadripole.

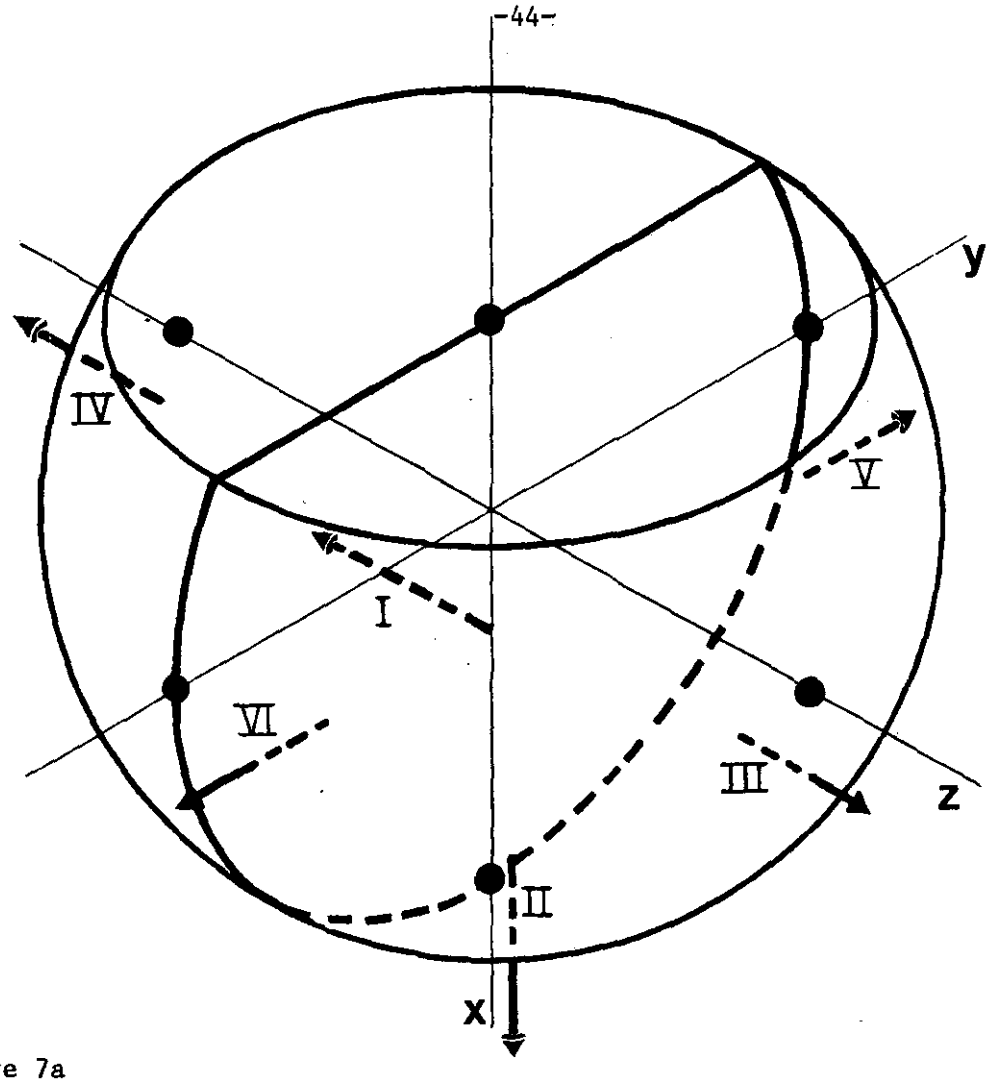

figure 7a

Positions of the discrete dipoles in the heart sphere. The exact coordinates are given in table 2. The positions of the dipoles are defined as the time averaged gravity points of the double layer activity concerned.

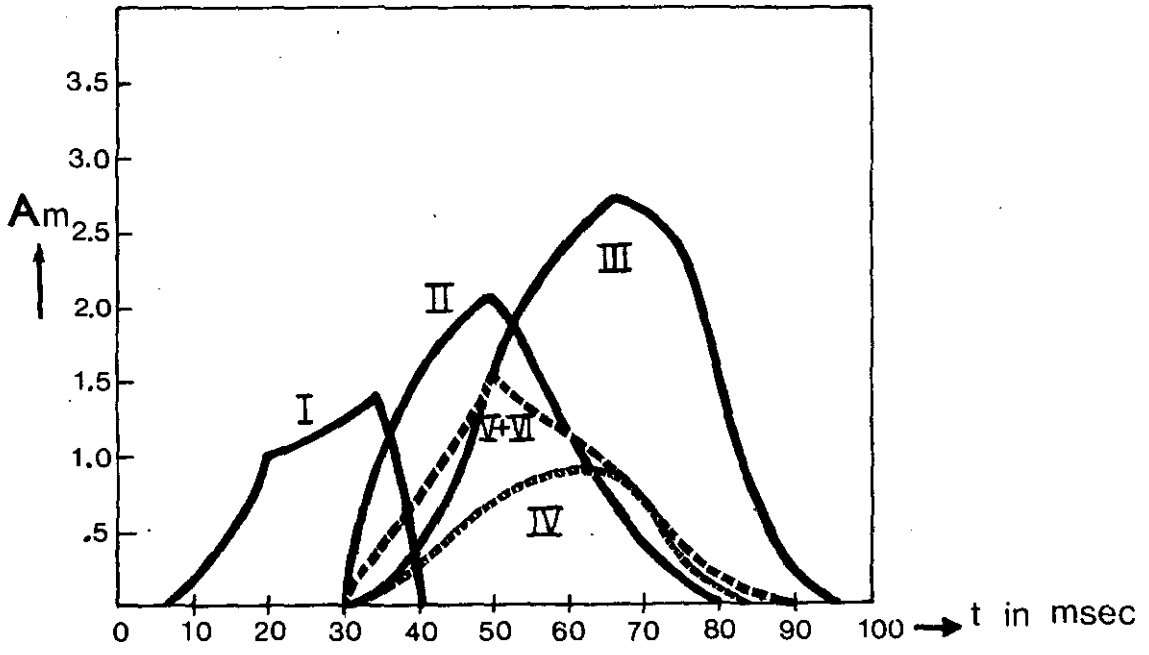

figure 7b

The strengths as a function of time of the different discrete dipoles. Each dipole represents a part of the heart activity and the strength moment of that special part.

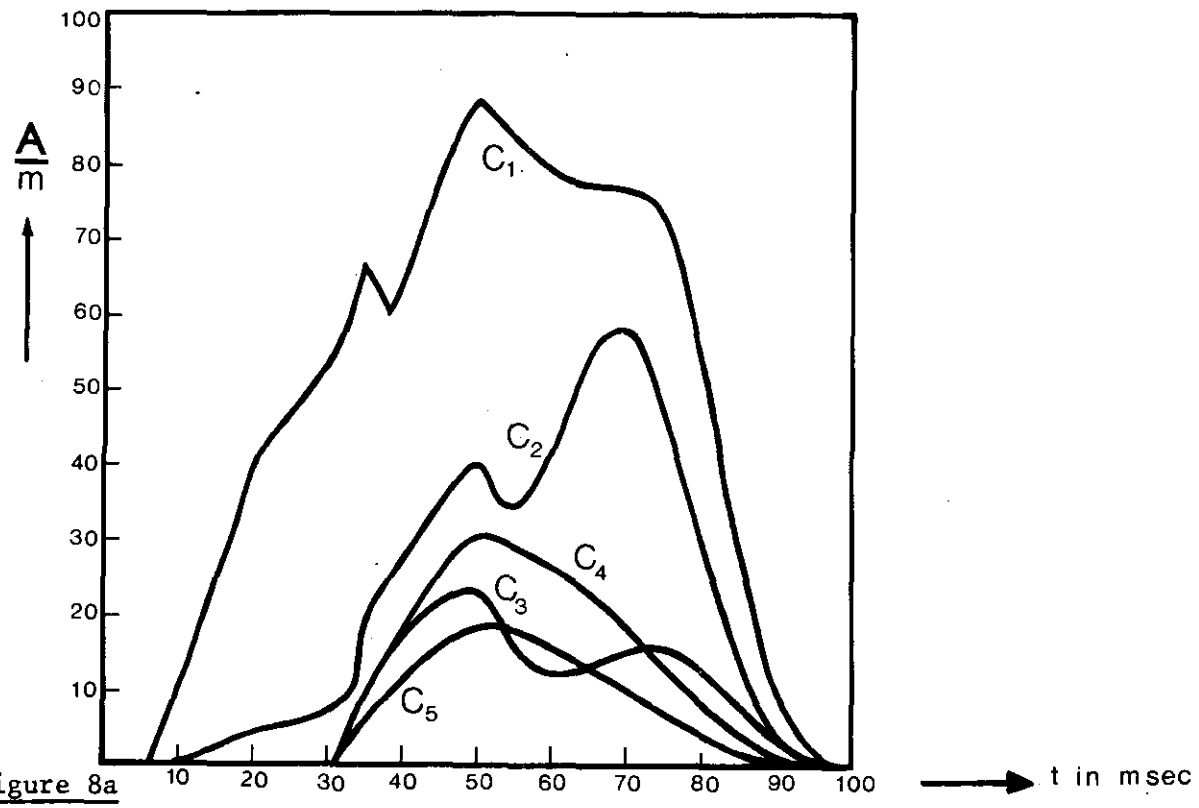

figure 8a

The multipole components in the RMS(Φ_{av}) of the potential on a concentric sphere (radius 2R) for the six dipole model.

$$\Phi_{av} = \sqrt{\sum_{n=1}^{\infty} c^2_{n6D}} \qquad c^2_{n6D} = \sum_{m=o}^{n} \frac{1}{(2R)^{2n+2}} a^2_{nm6D} \frac{1}{2n+1} \frac{(n+m)!}{(n-m)!} \frac{1}{2-\delta^o_m}$$

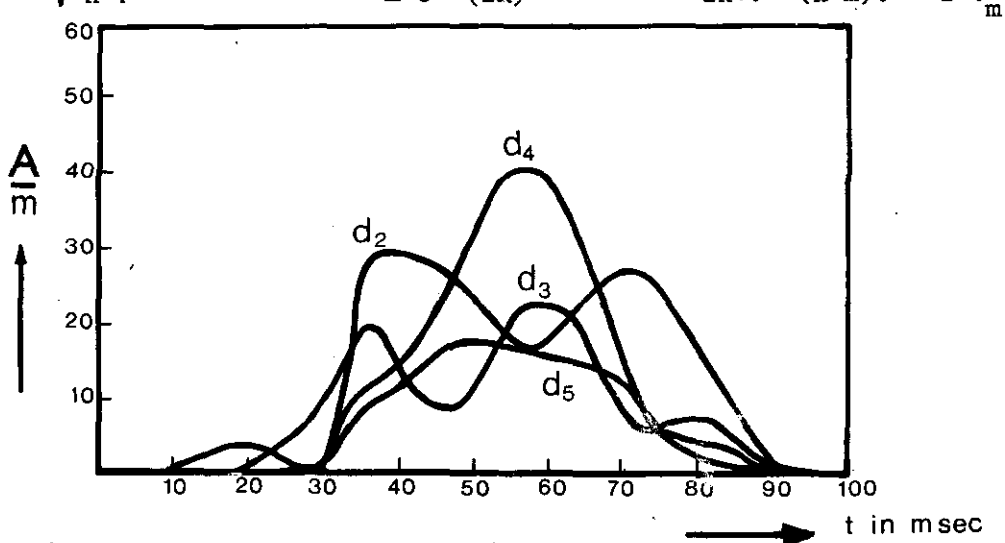

figure 8b

The differences in multipole components in the RMS of the potential differences on a sphere (2R) between the string model and the six dipole model.

$$d^2_n = \sum_{m=0}^{n} \frac{1}{(2R)^{2n+2}} (a_{nms} - a_{nm6D})^2 \frac{1}{2n+1} \frac{(n+m)!}{(n-m)!} \frac{1}{2-\delta^o_m}$$

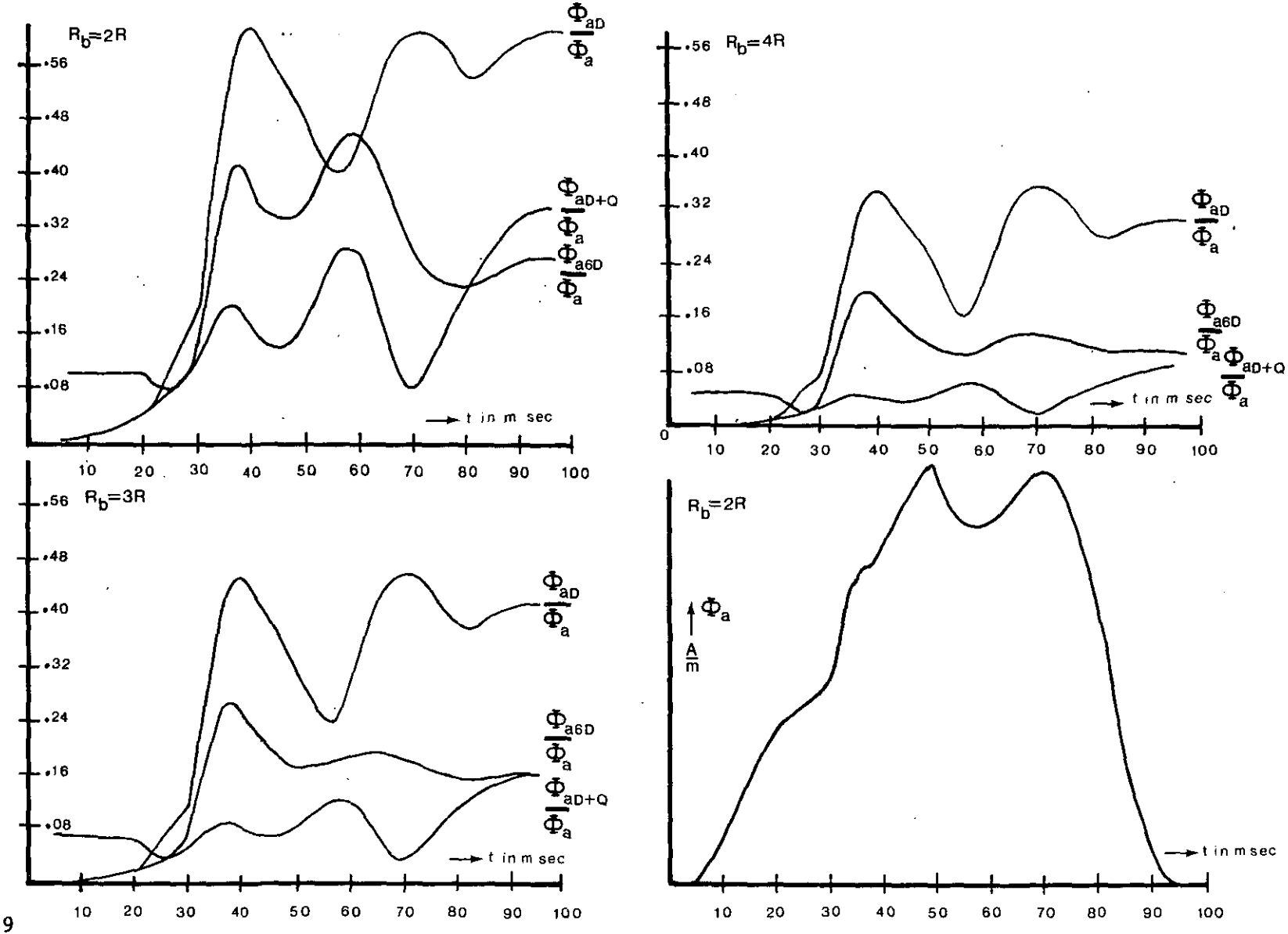

figure 9

Relative errors of the different models with respect to the string model. Φ_a is the RMS value of the potential on the spherical boundary (radius 2R) for the string model. Φ_{aD}, Φ_{aD+Q} and Φ_{a6D} are the RMS values of the potential differences on a spherical boundary (radius R6) between the respective models and the string model

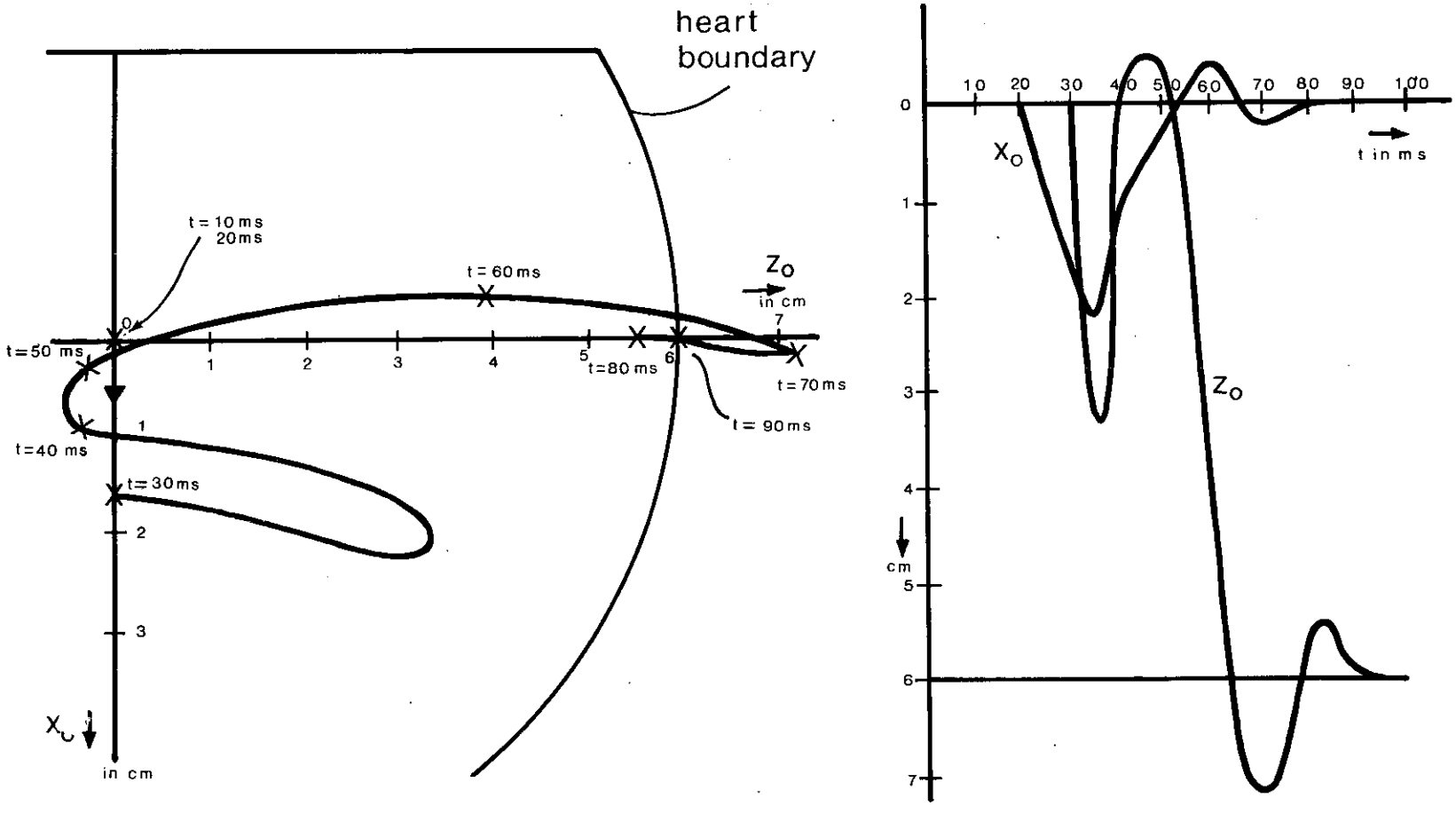

figure 10

The trajectory of the origin of the multipole expansion, which is optimal according to the definition of Geselowitz (ref. 25).

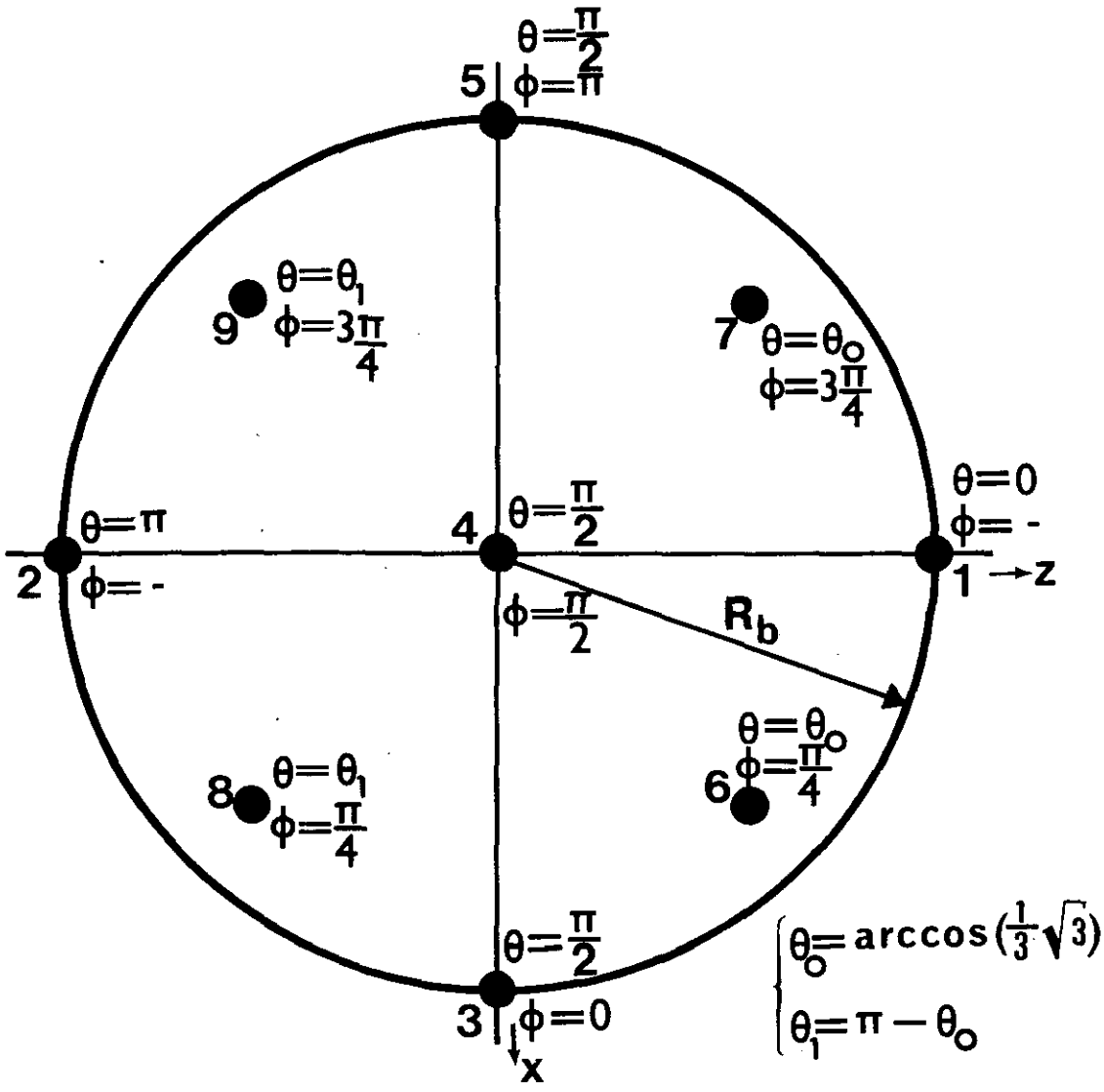

figure 11

Projection of the electrode positions on the x-z-plane. (y < 0).

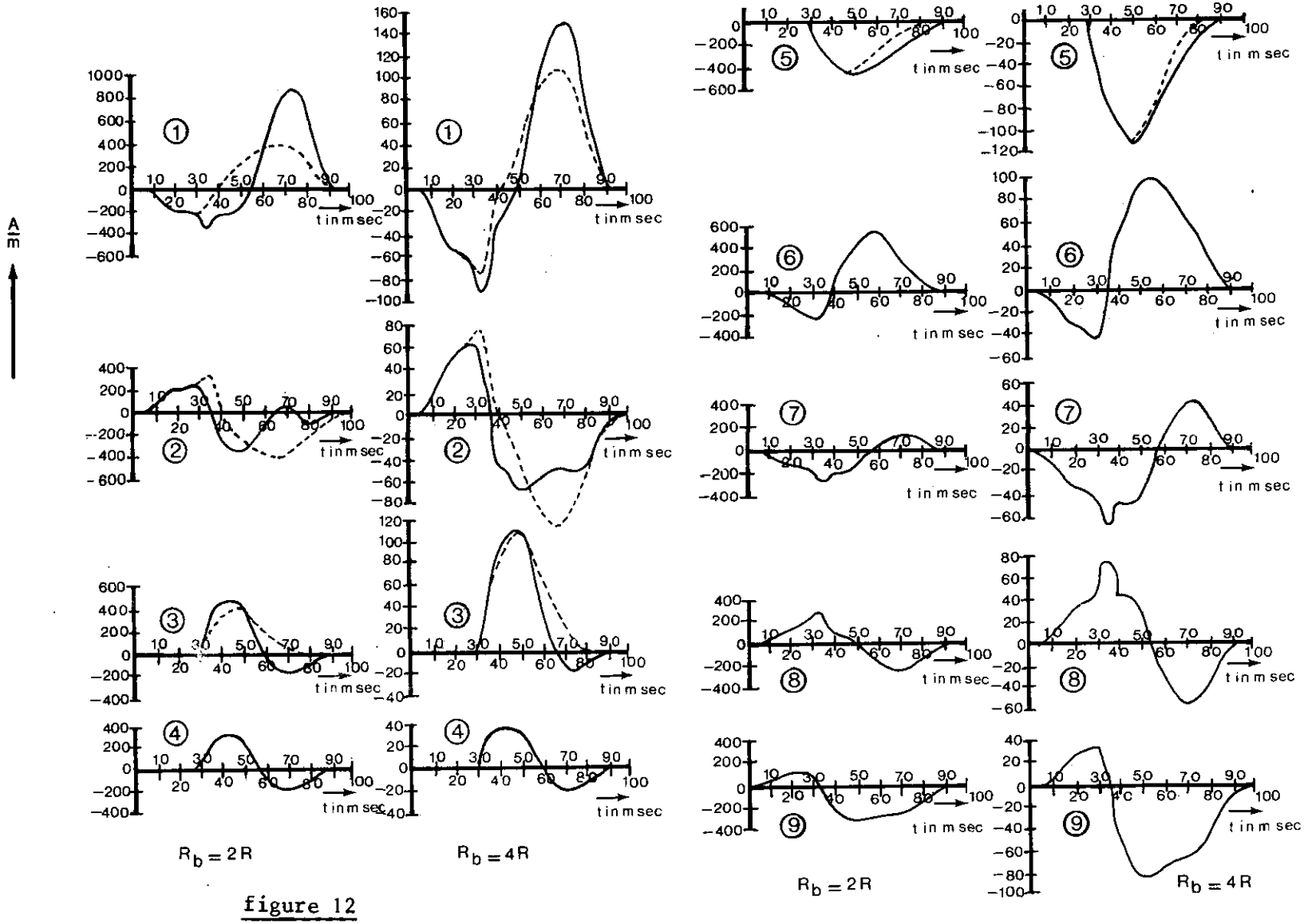

figure 12

Potentials as a function of time for the nine electrodes.

The radius of the spherical boundary is chosen to be 2R or 4R.

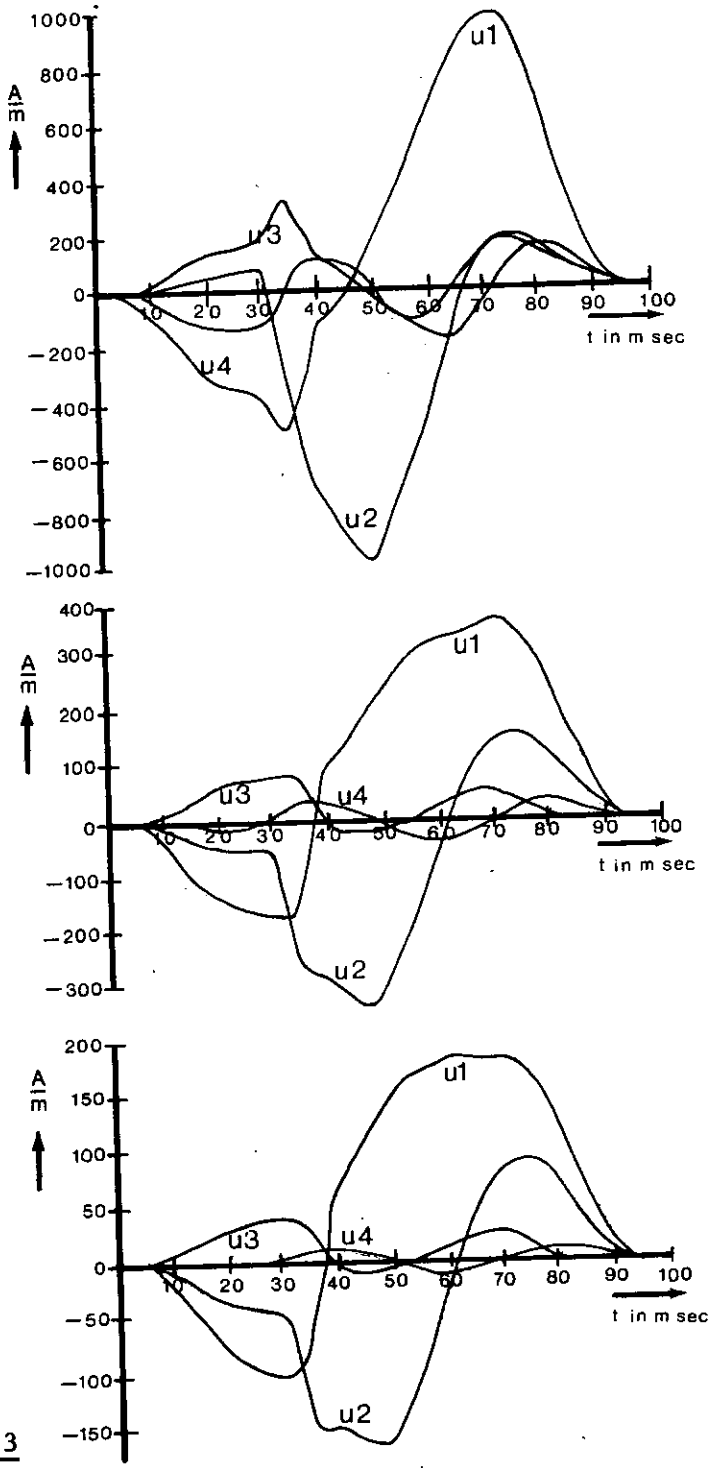

$$\sqrt{\frac{\sum_{j=p+1}^{9}\lambda_i}{\sum_{i=1}^{9}\lambda_i}}$$ in %

	%			
u1	54	26	18	4
u2	39			
u3	4			
u4	3			
u5	0			
u6	0			
u7	0			$R_b = 2R$
u8	0			
u9	0			
u1	61	18	9	1
u2	36			
u3	2			
u4	1			
u5	0			
u6	0			
u7	0			$R_b = 3R$
u8	0			
u9	0			
u1	64	14	5	1
u2	34			
u3	2			
u4	0			
u5	0			
u6	0			
u7	0			$R_b = 4R$
u8	0			
u9	0			

$$\frac{\lambda_i}{\sum_{j=1}^{9}\lambda_j}$$

figure 13

The most important intrinsic components of the nine electrod signals on spheres with radii of 2R, 3R and 4R.
The relative error made if only p intrinsic components are used, is also given as well as the relative energy of each intrinsic component.

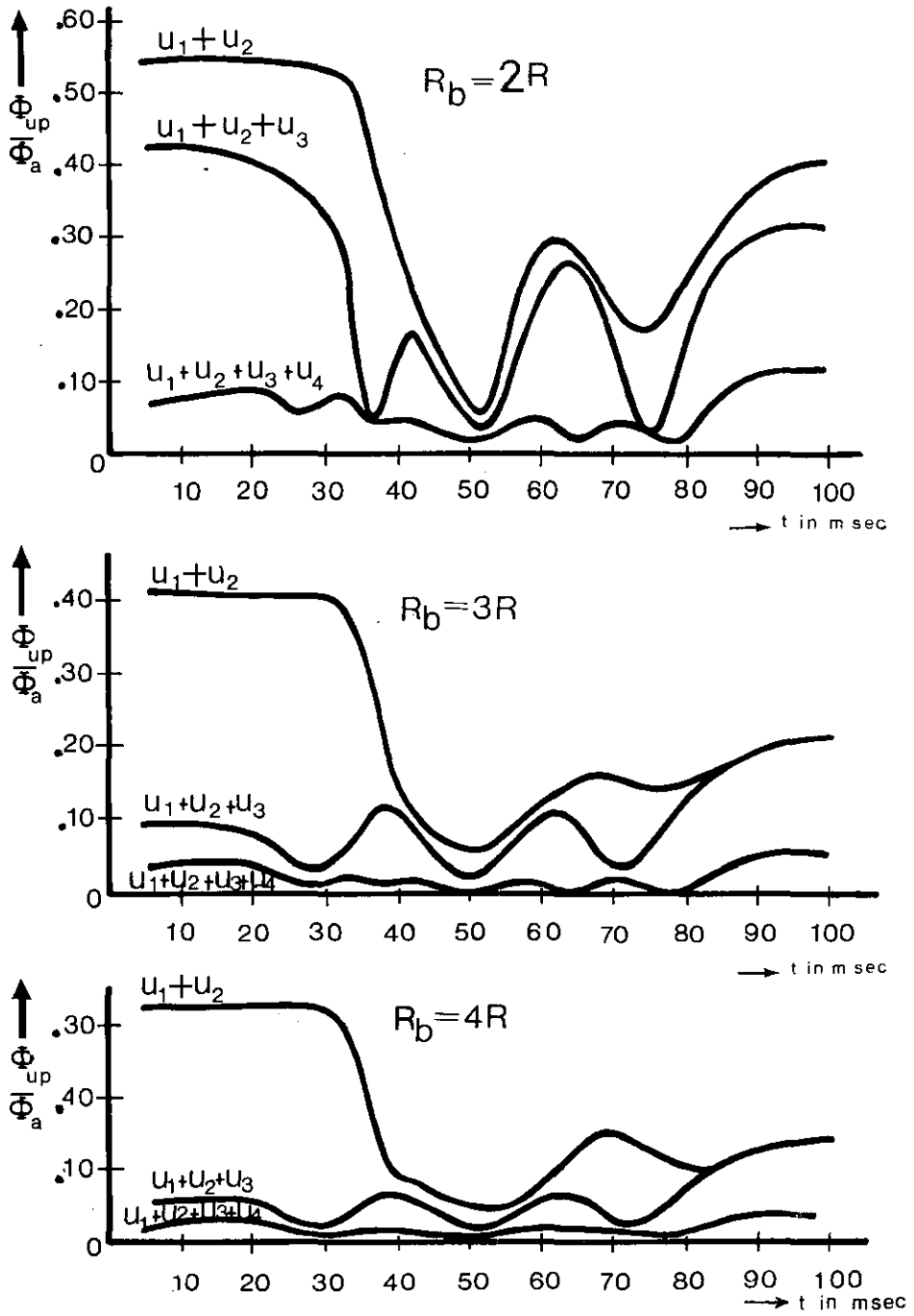

figure 14

The relative error for a reconstruction of the nine electrode signals by means of the p most significant intrinsic components. p = 2, 3 or 4. The radius of the spherical boundary is 2R, 3R or 4R.

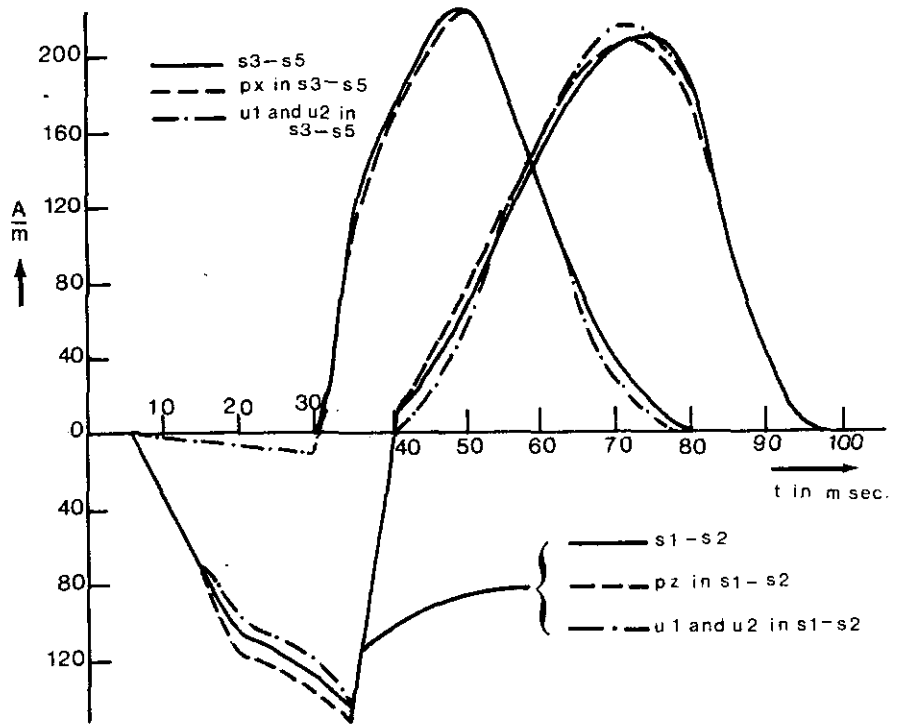

figure 15a

The potential difference between electrodes 1 and 2 : s1 - s2. The contribution to this potential difference of the dipole component p_z and the summed contribution of intrinsic components u_1 and u_2. The same for respectively s3 - s5, p_x and u1, u2.

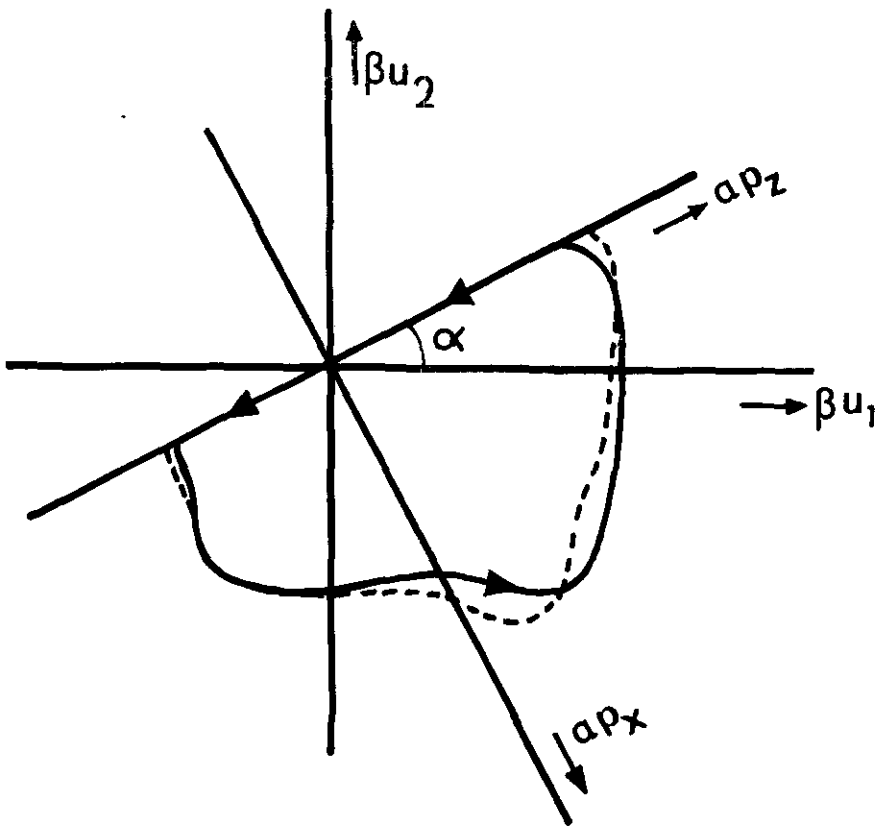

figure 15b

Illustrations of the correspondence between the dipole components p_x, p_z and the first two intrinsic components. Weighted with suitable coefficients α and β for appropriate amplitude, it can be seen, that a single rotation transforms the one set time functions into the other.

$\beta u_1 (\beta u_2)$ is the dotted line

$\alpha p_x (\alpha p_z)$ is the full time

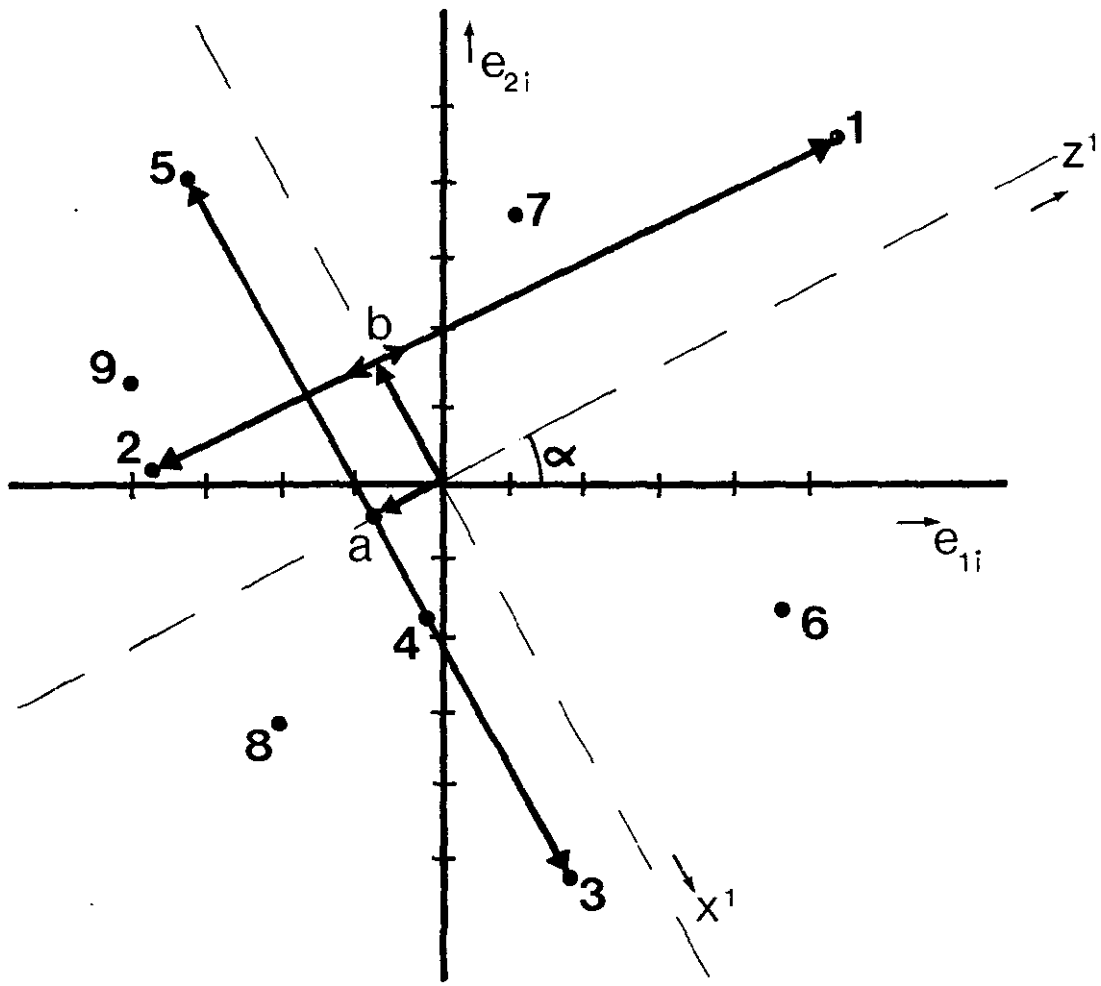

figure 16

The image space with respect to the two main intrinsic components. Along the x^1 and z^1 axis, on finds the coefficients of the dipole components p_x and p_z respectively. The numbers correspond to the electrodes.

EINDHOVEN UNIVERSITY OF TECHNOLOGY

THE NETHERLANDS

DEPARTMENT OF ELECTRICAL ENGINEERING

TH-Reports:

1. Dijk, J., M. Jeuken and E.J. Maanders
   AN ANTENNA FOR A SATELLITE COMMUNICATION GROUND STATION (PROVISIONAL ELECTRICAL DESIGN). TH-report 60-E-01. March 1968. ISBN 90 6144 001 7.
2. Veefkind, A., J.H. Blom and L.H.Th. Rietjens.
   THEORETICAL AND EXPERIMENTAL INVESTIGATION OF A NON-EQUILIBRIUM PLASMA IN A MHD CHANNEL. TH-report 68-E-2. March 1968. ISBN 90 6144 002 5.
   Submitted to the Symposium on a Magnetohydrodynamic Electrical Power Generation, Warsaw, Poland, 24-30 July, 1968.
3. Boom, A.J.W. van den and J.H.A.M. Melis.
   A COMPARISON OF SOME PROCESS PARAMETER ESTIMATING SCHEMES.
   TH-report 68-E-03. September 1968. ISBN 90 6144 003 3.
4. Eykhoff, P., P.J.M. Ophey, J. Severs and J.O.M. Oome.
   AN ELECTROLYTIC TANK FOR INSTRUCTIONAL PURPOSES REPRESENTING THE COMPLEX-FREQUENCY PLANE. TH-report 68-E-04. September 1968. ISBN 90 6144 004 1.
5. Vermij, L. and J.E. Daalder.
   ENERGY BALANCE OF FUSING SILVER WIRES SURROUNDED BY AIR.
   TH-report 68-E-05. November 1968. ISBN 90 6144 005 X.
6. Houben, J.W.M.A. and P. Massee.
   MHD POWER CONVERSION EMPLOYING LIQUID METALS.
   TH-Report 69-E-06. February 1969. ISBN 90 6144 006 8.
7. Heuvel, W.M.C. van den and W.F.J. Kersten.
   VOLTAGE MEASUREMENT IN CURRENT ZERO INVESTIGATIONS.
   TH-Report 69-E-07. September 1969. ISBN 90 6144 007 6.
8. Vermij, L.
   SELECTED BIBLIOGRAPHY OF FUSES.
   TH-Report 69-E-08. September 1969. ISBN 90 6144 008 4.
9. Westenberg, J.Z.
   SOME IDENTIFICATION SCHEMES FOR NON-LINEAR NOISY PROCESSES.
   TH-Report 69-E-09. December 1969. ISBN 90 6144 009 2.
10. Koop, H.E.M., J. Dijk and E.J. Maanders.
    ON CONICAL HORN ANTENNAS.
    TH-Report 70-E-10, February 1970. ISBN 90 6144 010 6.
11. Veefkind, A.
    NON-EQUILIBRIUM PHENOMENA IN A DISC-SHAPED MAGNETOHYDRODYNAMIC GENERATOR.
    TH-Report 70-E-11. March 1970. ISBN 90 6144 011 4.
12. Jansen, J.K.M., M.E.J. Jeuken and C.W. Lambrechtse.
    THE SCALAR FEED.
    TH-Report 70-E-12. December 1969. ISBN 90 6144 012 2
13. Teuling, D.J.A.
    ELECTRONIC IMAGE MOTION COMPENSATION IN A PORTABLE TELEVISION CAMERA.
    TH-Report 70-E-13. 1970. ISBN 90 6144 013 0.
14. Lorencin, M.
    AUTOMATIC METEOR REFLECTIONS RECORDING EQUIPMENT.
    TH-Report 70-E-14. November 1970. ISBN 90 6144 014 9.
15. Smets, A.J.
    THE INSTRUMENTAL VARIABLE METHOD AND RELATED IDENTIFICATION SCHEMES.
    TH-Report 70-E-15. November 1970. ISBN 90 6144 015 7.
16. White, Jr., R.C.
    A SURVEY OF RANDOM METHODS FOR PARAMETER OPTIMIZATION.
    TH-Report 70-E-16. February 1971. ISBN 90 6144 016 5.
17. Talmon, J.L.
    APPROXIMATED GAUSS-MARKOV ESTIMATORS AND RELATED SCHEMES.
    TH-Report 71-E-17. February 1971. ISBN 90 6144 017 3.
18. Kalášek, V.
    MEASUREMENT OF TIME CONSTANTS ON CASCADE D.C. ARC IN NITROGEN.
    TH-Report 71-E-18. February 1971. ISBN 90 6144 018 1.
19. Hosselet, L.M.L.F.
    OZONBILDUNG MITTELS ELEKTRISCHER ENTLADUNGEN.
    TH-Report 71-E-19. March 1971. ISBN 90 6144 019 X.
20. Arts, M.G.J.
    ON THE INSTANTANEOUS MEASUREMENT OF BLOODFLOW BY ULTRASONIC MEANS.
    TH-Report 71-E-20. May 1971. ISBN 90 6144 020 3.
21. Roer, Th. G. van de
    NON-ISO THERMAL ANALYSIS OF CARRIER WAVES IN A SEMICONDUCTOR.
    TH-Report 71-E-21. August 1971. ISBN 90 6144 021 1.
22. Jeuken, P.J., C. Huber and C.E. Mulders.
    SENSING INERTIAL ROTATION WITH TUNING FORKS.
    TH-Report 71-E-22. September 1971. ISBN 90 6144 022 X.

23. Dijk, J. and E.J. Maanders.
APERTURE BLOCKING IN CASSEGRAIN ANTENNA SYSTEMS. A REVIEW.
TH-Report 71-E-23. September 1971. ISBN 90 6144 023 8

24. Kregting, J. and R.C. White, Jr.
ADAPTIVE RANDOM SEARCH.
TH-Report 71-E-24. October 1971. ISBN 90 6144 024 6

25. Damen, A.A.H. and H.A.L. Piceni.
TH-Report 71-E-25. October 1971. ISBN 90 6144 025 4

26. Bremmer, H.
A MATHEMATICAL THEORY CONNECTING SCATTERING AND DIFFRACTION PHENOMENA INCLUDING BRAGG-TYPE INTERFERENCES.
TH-Report 71-E-26. December 1971. ISBN 90 6144 026 2.

27. Bokhoven, W.M.G. van
METHODS AND ASPECTS OF ACTIVE-RC FILTERS SYNTHESIS.
TH-Report 71-E-27. 10 December 1970. ISBN 90 6144 027 0.

28. Boeschoten, F.
TWO FLUIDS MODEL REEXAMINED.
TH-Report 72-E-28. March 1972. ISBN 90 6144 028 9.

29. Rietjens, L.H.Th.
REPORT ON THE CLOSED CYCLE MHD SPECIALIST MEETING. WORKING GROUP OF THE JOINT ENEA: IAEA INTERNATIONAL MHD LIAISON CROUP AT EINDHOVEN, THE NETHERLANDS. September 20, 21 and 22, 1971.
TH-Report 72-E-29. April 1972. ISBN 90 6144 029 7

30. C.C.M. van Kessel and J.W.M.A. Houben.
LOSS MECHANISMS IN AN MHD-GENERATOR.
TH-Report 72-E-30. June 1972. ISBN 90 6144 030 0.

31. A. Veefkind.
CONDUCTING GUIDS TO STABILIZE MHD-GENERATOR PLASMAS AGAINST IONIZATION INSTABILITIES. TH-Report 72-E-31. October 1972. ISBN 90 6144 031 9.

32. J.E. Daalder and C.W.M. Vos.
DISTRIBUTION FUNCTIONS OF THE SPOT-DIAMETER FOR SINGLE- AND MULTI-CATHODE DISCHARGES IN VACUUM. TH-Report 73-E-32. January 1973. ISBN 90 6144 032 7.

33. J.E. Daalder.
JOULE HEATING AND DIAMETER OF THE CATHODE SPOT IN A VACUUM ARC.
TH-Report 73-E-33. January 1973. ISBN 90 6144 033 5.

34. Huber, C.
BEHAVIOUR OF THE SPINNING GYRO ROTOR.
TH-Report 73-E-34. February 1973. ISBN 90 6144 034 3.

35. Boeschoten, F.
THE VACUUM ARC AS A FACILITY FOR RELEVANT EXPERIMENTS IN FUSION RESEARCH.
TH-Report 73-E-35, February 1973, ISBN 90 6144 035 1.

36. Blom, J.A.
ANALYSIS OF PHYSIOLOGICAL SYSTEMS BY PARAMETER ESTIMATION TECHNIQUES.
73-E-36. 1973. ISBN 90 6144 036 X

37. Lier, M.C. van and R.H.J.M. Otten.
AUTOMATIC WIRING DESIGN.
TH-reprot 73-E-37. May 1973. ISBN 90 6144 037 8

38. Andriessen, F.J.
CALCULATION OF RADIATION LOSSES IN CYLINDRICAL SYMMETERICAL HIGH PRESSURE DISCHARGES BY MEANS OF A DIGITAL COMPUTER.
TH-report 73-E-38. October 1973. ISBN 90 6144 038 6

39. Dijk, J., C.T.W. van Diepenbeek, E.J. Maanders and L.F.C. Thurlings.
THE POLARIZATION LOSSES OF OFFSET ANTENNAS.
TH-report 73-E-39. June 1973. ISBN 90 6144 039 4.

40. Goes, W.P.
SEPARATION OF SIGNALS DUE TO ARTERIAL AND VENOUS BLOODFLOW, IN THE DOPPLER SYSTEM, THAT USES CONTINUOUS ULTRASOUND.
TH-report 73-E-40. September 1973. ISBN 90 6144 040 8